GNL3 regulates replication origin firing and protects stalled replication forks

Rana Lebdy[1,2], Marine Canut[1], Julie Patouillard[1], Jean-Charles Cadoret[3], Anne Letessier[4], Josiane Ammar[1], Jihane Basbous[1], Serge Urbach[5], Benoit Miotto[4], Angelos Constantinou[1], Raghida Abou Merhi[2 *] and Cyril Ribeyre[1,6*]

[1]Institut de Génétique Humaine (UMR9002), CNRS, Université de Montpellier.
141, Rue de la Cardonille, 34396 Montpellier Cedex 5, France

[2]Faculty of Sciences, Genomics and Surveillance Biotherapy (GSBT) Laboratory, R. Hariri Campus, Lebanese University, Hadath 1003, Lebanon.

[3]Université Paris Cité, CNRS, Institut Jacques Monod, F-75006 Paris, France
15 rue Hélène Brion,75013 Paris, France

[4]Université Paris Cité, Institut Cochin, INSERM, CNRS, F-75014 PARIS, France
22, rue Mechain, 75014 Paris, France

[5]Institut de Génomique Fonctionnelle, CNRS UMR 5203, Inserm U1191, Université de Montpellier.
141, Rue de la Cardonille, 34094 Montpellier Cedex 5, France

[6]Lead contact

*Correspondence: raboumerhi@ul.edu.lb or cyril.ribeyre@igh.cnrs.fr

Summary

DNA replication by the replisome requires specific proteins that protect replication forks and so prevent the formation of DNA lesions that may damage the genome. Here, we show that human GNL3/nucleostemin, a GTP-binding protein localized in the nucleolus and the nucleoplasm, is a new component of the replisome. Depletion of GNL3 reduces fork speed but increases replication origin firing. When subjected to replication stress, the nascent DNA of GNL3-depleted cells undergoes nuclease-dependent resection, a source of DNA lesions. Inhibition of origin firing decreases this resection, indicating that the increased replication origin firing seen upon GNL3 depletion mainly accounts for the observed DNA resection. We show that GNL3 and DNA replication initiation factor ORC2 interact in the nucleolus, and that GNL3 regulates ORC2 subnuclear localization. The accumulation of GNL3 in the nucleolus is thus required to limit DNA resection in response to replicative stress, potentially through the regulation of ORC2 functions.

Keywords

GNL3, DNA replication, DNA replication stress, ORC2, DNA resection, origin firing

Introduction

In all cells, DNA replication must occur precisely before their division to ensure faithful transmission of the genome. In humans, accurate DNA replication is particularly important for stem cells and to prevent premature aging and/or cancer (Macheret and Halazonetis, 2015; Schumacher et al., 2021). Replication must occur correctly in space and time to ensure that the whole genome is copied entirely once per cell cycle with no under-replicated or over-replicated regions. Moreover, the replication forks – the sites at which the replication machinery (the replisome) replicates DNA – must be free of impediments that perturb their progression because collapsed replication forks can result in DNA lesions.

DNA replication initiates from specific sites distributed all over the genome, called replication origins (Fragkos et al., 2015; Mechali, 2010). Initiation of replication is a two-step process. First, the origins are 'licensed' for replication by binding of the origin recognition complex (ORC, composed of six subunits, ORC1–6) and the replicative helicase MCM2–7, which forms the pre-replicative complex. Second, origin firing (the start of DNA synthesis) requires activation of cyclin-dependent kinases and CDC7/DBF4 kinases. Although the ORC complex is mainly responsible for initiating DNA replication, it also has other functions. For example, one of the ORC subunits, ORC2, plays structural roles independent of the ORC complex, which may impact DNA replication indirectly (Huang et al., 2016; Prasanth et al., 2004; Shimada and Gasser, 2007).

After DNA replication starts, the progression of the replisome may be perturbed by factors of endogenous and exogenous origin that induce replication stress (Lambert and Carr, 2013). The main pathway activated to prevent fork collapse and genomic instability, the ATR–Chk1 checkpoint, prevents further progress through S phase, thus providing time for stalled forks to be stabilized to avoid formation of DNA lesions (Zeman and Cimprich, 2014). Many other proteins, for example BRCA1, protect stalled forks by preventing the action of specific nucleases like MRE11 or CtIP (Berti et al., 2020; Liao et al., 2018; Rickman and Smogorzewska, 2019). ATR–Chk1 also maintains genomic stability by limiting the firing of replication origins in response to replication stress (Blow et al., 2011; Courtot et al., 2018; Toledo et al., 2013). WEE1, a kinase that limits entry into mitosis by inhibiting CDK1, acts in a similar way (Beck et al., 2012; Moiseeva et al., 2019; Toledo et al., 2013).

We previously used the iPOND (isolation of proteins on nascent DNA) method coupled with mass spectrometry (iPOND-MS) to identify novel factors associated with replication forks (Lossaint et al., 2013; Ribeyre et al., 2021; Ribeyre et al., 2016). Here, we used an siRNA screen to identify those novel factors

whose depletion increases the number of DNA lesions in response to replication stress. The protein whose depletion had the greatest effect was GNL3 (also known as nucleostemin), a GTP-binding protein localized mainly in the nucleolus which is highly expressed in stem cells and cancer cell lines (Tsai and McKay, 2002). Previous studies found that GNL3 depletion leads to activation of the DNA damage response during S phase (Lin et al., 2013; Meng et al., 2013; Yamashita et al., 2013). GNL3 is recruited to DNA double-stand breaks (DSBs), and its depletion prevents RAD51 – a key protein for DSBs repair by homologous recombination – from being recruited at DSBs and hydroxyurea (HU)-induced lesions (Lin et al., 2013; Meng et al., 2013). Consistent with this, GNL3-depleted cells are more sensitive to HU (Lin et al., 2014) and are less able to repair DSBs by homologous recombination (Meng et al., 2013). The current model suggests that GNL3 in the nucleoplasm maintains genome stability in S phase by being recruited to DNA lesions in order to stabilize RAD51 (Tsai, 2014). The precise functions of GNL3 in S phase, its role in DNA replication and genome stability, are poorly understood, however. In this report, we demonstrate that GNL3 is constitutively associated with nascent DNA in human cells and is required to protect stalled replication forks by limiting replication origins firing.

Results

GNL3 is a new replisome component

We reported previously our use of the iPOND method to identify novel factors associated with replication forks (Ribeyre et al., 2021). Briefly, we pulse-labelled newly synthesized DNA in Hela S3 cells with 5-ethynyl-2'-deoxyuridine (EdU, a nucleoside analogue of thymidine that can be labelled by Click chemistry) or pulsed with EdU then chased for two hours with thymidine, then we purified the proteins associated with EdU (Figure 1A). Those proteins that were significantly enriched in the pulse-labelled samples when compared to the chase were defined as components of the replisome (Ribeyre et al., 2021). These components included many proteins that were not previously known to be associated with nascent DNA. To select candidates for further analysis, we designed an orthogonal approach based on a mini screen using 25 individual endoribonuclease-prepared siRNAs (esiRNAs; against 24 candidates plus a negative control esiRNA against EGFP). We reasoned that if these proteins are important for DNA replication, their depletion should increase the number of DNA lesions upon replication stress. We analyzed DNA lesions by quantifying the amount of γH2A.X phosphorylation after 4 hours of replication stress due to treatment with 1 μM camptothecin (CPT, an inhibitor of DNA topoisomerase 1). Briefly, HCT116 cells growing in 96 well plates were transfected with each of the 25 esiRNAs. Forty-eight hours after transfection, the cells were treated for 4 hours with 1 μM CPT and the amount of γH2A.X in the nucleus (seen by staining with DAPI) was analyzed by immunofluorescence microscopy using a Celigo high-throughput microscope (Figure S1A). We ranked the effects of the 25 esiRNAs based on the amount of γH2A.X and found that GNL3 ranked highest, suggesting that it may be important to tolerate replication stress (Figure S1B).

Using the iPOND–MS data (Ribeyre et al., 2021), we calculated the logRatio of GNL3 in the pulse and the chase samples and found that it had a similar profile than known replisome components such as PCNA, RFC1 and FEN1 (Figure 1B). Also, by western blotting the iPOND proteins, we observed that GNL3, like PCNA, was associated with EdU only when the Click reaction was performed and was not found in the chase (Figure 1C), further supporting the conclusion that it is a replisome component. To confirm that GNL3 is localized at replication forks, we performed proximity ligation assays (PLAs) between GNL3 and the EdU-containing nascent DNA Click-labeled with biotin, using antibodies against GNL3 and biotin to identify foci where the two antigens are in close proximity. We found many foci showing the proximity of GNL3 to nascent DNA in the nuclei of normal cells; by contrast, the number of foci was much decreased when GNL3 was depleted (Figure 1D, 1E) or when EdU was not Click-labeled with biotin (Figure 1F). We conclude from these data that GNL3 is new replisome component.

GNL3 depletion increases firing of replication origins

If GNL3 is a component of the replisome, its depletion might be expected to have an impact on the cell cycle. We found no obvious effect of GNL3 depletion, however, either on the distribution of cells in various phases of the cell cycle whether in an unsynchronized population (Figure S2A) or in a population synchronized with a thymidine block (Figure S2B). To confirm this conclusion, we measured the length of S phase by examining the timing of entry into mitosis after a thymidine block, as indicated by phosphorylation of histone H3 on Ser 10 (Prigent and Dimitrov, 2003). Confirming that the length of S phase was unaffected by GNL3 depletion, no sign of early mitotic entry was detected 8 hours after release (Figure S2C). Ten hours after release, however, we noticed a small increase in the percentage of pH3S10-positive cells in GNL3-depleted cells when compared to the control, suggesting the cells accumulate in mitosis in the absence of GNL3, a phenomenon observed also in breast cancer cells lacking GNL3 (Lin et al., 2014). In those cells, loss of GNL3 increased the number of foci containing the DNA damage response protein 53BP1 (Lin et al., 2014; Yamashita et al., 2013), potentially an indicator of incomplete replication due to replication stress (Harrigan et al., 2011). Cells undergoing replication stress have been observed to continue replicating their DNA in early mitosis, a phenomenon known as mitotic DNA synthesis (MiDAS; (Minocherhomji et al., 2015). To test whether GNL3 depletion induces MiDAS, we synchronized cells with thymidine, released them for 8 hours and then labelled nascent DNA for 15 min with EdU (Figure S2D). GNL3 depletion increased the number of mitotic cells with an EdU signal by about two-fold (Figure S2E), indicating that these cells enter mitosis with incompletely replicated DNA, suggesting problems during DNA replication. To determine whether GNL3 depletion has a global impact on DNA synthesis during S phase, we measured incorporation of the thymidine analogue iodo-deoxyuridine (IdU) and found it increased in comparison to control cells (Figure 2A, 2B, Figure S2F). Since the length of S phase is not affected by GNL3 depletion, this may reflect a change in the number of active replication origins. To test this, we isolated the chromatin from cells depleted of GNL3 and from control cells and analyzed the presence of markers of origin firing by western blotting. We found more CDC45, MCM2 phosphorylated at Ser 40/41 (pMCM2 S40/41) and PCNA in the chromatin fraction of cells depleted of GNL3 than in control cells (Figure 2C, 2D) indicating that more origins are firing in the absence of GNL3. To confirm this finding by using another approach, we used DNA combing (Figure 2E): we labelled the cells with IdU for 20 min and then with another thymidine analogue, chloro-deoxyuridine (CldU), for 20 min and observed that GNL3 depletion reduced fork velocity by about 25% (Figure 2F, Figure S2G). This indicates that the increased IdU incorporation in GNL3-depleted cells is not due to increased fork velocity but that it might reflect more replication forks. To investigate this possibility, we determined the number of forks per

megabase of combed DNA by using a highly accurate assay for global instant fork density (Bialic et al., 2015), which reflects the density of fired replication origins. A significant increase in the number of forks per megabase in GNL3-depleted cells indicated that indeed more origins fire in absence of GNL3 than in control cells (Figure 2G). To investigate whether GNL3 affects the firing of replication origins globally or only at specific regions, as does RIF1 (Yamazaki et al., 2012), we analyzed the effect of GNL3 depletion on replication timing. As expected from previous studies (Cornacchia et al., 2012; Yamazaki et al., 2012), depletion of RIF1 had a substantial impact on replication timing; some regions were delayed and others advanced when compared to the control (Figure S2H). GNL3 depletion, by contrast, had little or no effect on replication timing (Figure 2H). We conclude that GNL3 depletion increases the firing of replication origins globally without affecting the replication timing.

GNL3 prevents DNA resection at stalled replication forks

GNL3 depletion leads to activation of the DNA damage response during S phase and GNL3-depleted cells are more sensitive than control cells to HU, an inducer of replication stress (Lin et al., 2013; Lin et al., 2014; Meng et al., 2013; Yamashita et al., 2013), suggesting a role in the response to replication stress. Indeed, we found more γH2A.X in the nucleus of CPT-treated cells depleted of GNL3 than in control cells (Figure S1B); therefore, we investigated further whether GNL3 regulates replication fork progression in the presence of CPT. To do so, we labelled cells for 30 min with IdU followed by labelling for 30 min with CldU in the presence or absence of 1 μM CPT and measured the length of both tracks to obtain the CldU/IdU ratio (Figure 3A). As expected, addition of CPT strongly reduced the CldU/IdU ratio, however, depletion of GNL3 had no additional impact (Figure 3A, Figure S3A). This indicates that GNL3 has no great influence on replication fork progression during brief treatments with CPT. When the cells were treated with CPT for 1, 2 and 4 hours (Figure S3B), CPT treatment induced rapid phosphorylation of the DNA damage response kinase Chk1 on Ser 345, as expected, however, the kinetics of its phosphorylation was not markedly affected by GNL3 depletion, further supporting our conclusion that GNL3 does not affect fork progression in response to CPT. By contrast, after 4 hours of treatment with CPT the level of phosphorylation of RPA on both Ser 33 and Ser 4/8 was higher in the absence of GNL3 than in the controls (Figure S3B). To determine if this effect was specific to CPT, we performed the same experiment but treated the cells with HU or etoposide (ETP), a topoisomerase 2 inhibitor. Treatment with 5 mM HU or 10 μM ETP induced phosphorylation of Chk1 on serine 345 in control cells but, as with CPT, no obvious difference was seen when GNL3 was depleted (Figure 3B and Figure S3C). Also, as with CPT, we observed stronger phosphorylation of RPA on Ser 33 and Ser 4/8 in the absence of GNL3 than in control cells after

4 hours treatment with HU (Figure 3B) and after 2 hours treatment with ETP (Figure S3C). Thus, we hypothesized that GNL3 depletion may not impact replication stress signaling through Chk1 but, rather, the stability of stalled replication forks, since RPA phosphorylation is a marker of DNA resection (Soniat et al., 2019). Several proteins, including BRCA1, BRCA2 and FANCD2, have been shown to protect nascent DNA from resection in response to replication stress (Rickman and Smogorzewska, 2019). To test if GNL3 protects nascent strand DNA, we sequentially labelled cells with IdU and CldU for 30 min each and then treated the cells with HU for 4 hours (Figure 3C). In the controls, the CldU/IdU ratio was close to 1, indicating that the nascent DNA was protected from extensive degradation, as expected. In cells depleted of GNL3, by contrast, the CldU/IdU ratio was significantly lower (Figure 3C, Figure S3D), indicating resection of the fork DNA by nuclease(s). Likewise, we saw similar effects in response to CPT (Figure S3E) and ETP (Figure S3F), consistent with the increased level of RPA phosphorylation induced by these agents in GNL3-depleted cells.

The resection observed in the absence of fork protectors is most probably initiated by the endonuclease activities of MRE11 and CtIP (Rickman and Smogorzewska, 2019). To test further the function of GNL3 as a fork protector, we depleted GNL3 and MRE11, or GNL3 and CtIP, and found that loss of the nucleases prevented the resection seen upon depletion of GNL3 alone (Figure 3D, Figure S3G, Figure S3H), further supporting our conclusion that GNL3 protects nascent strand degradation by nucleases. To show definitively that GNL3 protects against DNA resection at stalled replication forks, we depleted the endogenous GNL3 with a specific siRNA and complemented its function by expressing an siRNA-resistant, doxycycline(DOX)-inducible GNL3-FLAG gene in Flp-In T-Rex HeLa cells (Figure 3E). We treated these cells with HU and analyzed the level of resection by IdU and CldU incorporation, as before. Expression of siRNA-resistant GNL3-FLAG suppressed almost completely the increased resection due to GNL3 depletion (Figure 3F, Figure S3I).

Resection in the absence of GNL3 is a consequence of increasing origin firing

Other proteins known to protect replication forks – BRCA1, RAD51 and FANCD2, for example – accumulate on HU-stalled forks (Dungrawala et al., 2015; Lossaint et al., 2013; Zellweger et al., 2015), suggesting that they may protect them directly from the action of nucleases. To determine whether GNL3 protects stalled replication forks from nucleases in the same way, we again used iPOND to identify the proteins on nascent DNA. Cells were pulse labelled for 15 min with EdU and then chased for 2 hours with thymidine or with HU (Figure 4A). As we showed already (Figure 1C), the replisome components PCNA and GNL3 were enriched on nascent DNA after the pulse but not after the chase and, as expected, treatment with HU

enhanced recruitment of RAD51 (Figure 4B). By contrast, recruitment of GNL3 was strongly decreased in response to HU, as was PCNA (Figure 4B), indicating that GNL3 does not accumulate at stalled forks. This suggests that the ability of GNL3 to protect from resection might be indirect and possibly related to its role in inhibiting origin firing. If so, inhibiting origin firing might suppress the HU-induced resection observed upon GNL3 depletion (Figure 4C). To test this, we sequentially labelled cells with IdU and CldU for 30 min each and then treated them with HU for 4 hours in the presence of an inhibitor of CDC7 to inhibit replication origin firing. Resection was strongly decreased when CDC7 was inhibited, indicating that in the absence of GNL3 an excess of origin firing in response to HU accounts for the increased resection (Figure 4D, Figure S4A). Consistent with the decrease in DNA resection, CDC7 inhibition also decreased the phosphorylation of RPA on Ser4/8 (Figure 4E, Figure S4B).

BRCA1 is recruited to HU-stalled forks (Dungrawala et al., 2015) and its depletion increases DNA resection induced by HU (Schlacher et al., 2012), thus this protein is thought to protect stalled forks from resection by directly blocking nucleases. If this is the case, inhibition of CDC7 should have no effect on protection by BRCA1. To test this prediction, we depleted cells of BRCA1 and measured the level of resection in the absence or presence of the CDC7 inhibitor. As expected, depletion of BRCA1 increased resection; treatment with CDC7 inhibitor, however, did not decrease the level of resection (Figure 4F, Figure S4C, Figure S4D), confirming that the resection observed in the absence of BRCA1 is not a consequence of faulty origin firing. Thus, fork protection by BRCA1 differs mechanistically from fork protection by GNL3.

We saw above that in cells depleted of GNL3, replication stress resulted in both increased replication origin firing and increased resection. If this increased resection is a consequence of increased origin firing, other causes of increased replication origin firing should have a similar effect. Inhibition of ATR or WEE1, for example, increase replication origin firing (Beck et al., 2012; Moiseeva et al., 2017; Moiseeva et al., 2019) and WEE1 inhibition increases DNA resection in response to HU (Elbaek et al., 2022). We therefore tested the effect of inhibiting ATR or WEE1 on resection in response to HU by sequentially labelling cells with IdU and CldU and then treating them with HU for 4 hours, as before, but in the presence of an inhibitor of ATR or an inhibitor of WEE1 (Figure 4G, Figure S4E). As predicted, inhibition of ATR (Figure 4H, Figure S4F) or inhibition of WEE1 (Figure 4I, Figure S4G) increased resection in response to HU. Moreover, inhibiting the increased origin firing with an inhibitor of CDC7, partially reversed this effect. This experiment demonstrates that limiting the number of origins that fire is crucial to preventing resection in response to replication stress and supports our conclusion that the enhanced resection observed upon GNL3 depletion is a consequence of increased origin firing.

Nucleolar accumulation of GNL3 prevents resection

So far, we showed that GNL3 prevents DNA resection upon replication stress by limiting excessive activation of replication origins. However, since GNL3 is present both in the nucleoplasm and the nucleolus, we wished to determine what fraction of GNL3 is required for preventing resection in response to replication stress. To do so, we designed mutants of GNL3 lacking the different domains (Figure 5A) that were previously described (Tsai and McKay, 2002, 2005). We depleted endogenous GNL3 with a specific siRNA and expressed siRNA-resistant, DOX-inducible GNL3 mutants fused with FLAG in Flp-In T-Rex HeLa cells. GNL3-dB and GNL3-dC had a level of expression comparable to GNL3-WT, in contrast, GNL3-dG, GNL3-dI and GNL3-dA were expressed at lower level (Figure 5B). We next analyzed their localization using immunofluorescence with an antibody directed against FLAG (Figure 5C). As expected from previous work (Tsai and McKay, 2002, 2005), GNL3-dC, GNL3-dA and GNL3-dI were mainly localized in the nucleolus like GNL3-WT. Deletion of the G1 and G4 domains (GNL3-dG) prevents binding to GTP and altered its ability to be localized in the nucleolus (Huang et al., 2009; Tsai and McKay, 2005). Deletion of the B domain abolished its specific localization in the nucleolus leading to diffusion in the nucleoplasm. We then analyzed if expression of GNL3 mutants rescues the increased resection observed upon GNL3 depletion. As already shown (Figure 3F), expression of GNL3-WT almost completely suppressed the increased resection induced by GNL3 depletion (Figure 5D, Figure S5A). Similar results were observed for the expression of GNL3-dC, GNL3-dI or GNL3-dA (Figure 5D, Figure S5A). Interestingly, GNL3-dG did not fully complement the resection defect due to GNL3 depletion, however since this mutant is really unstable it is hard to draw any strong conclusions. In contrast, GNL3-dB, that has a level of expression comparable to GNL3-WT and GNL3-dC, did not fully complement the resection defect due to GNL3 depletion (Figure 5D, Figure S5A). Since GNL3-dB is diffusing in the nucleoplasm, on the contrary of GNL3-WT, GNL3-dC, GNL3-dI and GNL3-dA, we conclude that the accumulation of GNL3 in the nucleolus is required to prevent DNA resection. To confirm this result, we modulated GNL3-dB expression using different concentrations of DOX (Figure S5B) and observed that the diffusion in the nucleoplasm was dependent on DOX concentration (Figure S5C). Strikingly, we observed that the amount of resection was largely correlated with the level of expression of GNL3-dB (Figure S5D, S5E), confirming that the defect of resection observed is not due to a loss of function but to diffusion in the nucleoplasm. We conclude that the accumulation of GNL3 in the nucleolus prevents DNA resection in response to replication stress.

GNL3 interacts with ORC2 in the nucleolus

To understand how the presence of GNL3 in the nucleolus might influence replication origin firing, we used proximity-dependent biotinylation identification (BioID; (Roux et al., 2012)) to identify the proteins in proximity to GNL3 by mass spectrometry. We established a Flp-In T-Rex HEK293 cell line expressing a DOX-inducible GNL3 cDNA fused to the biotin ligase BirA and FLAG. Upon induction with DOX for 16 hours, we observed by immunofluorescence microscopy GNL3-BirA-FLAG mainly in the nucleolus (Figure S6A). Moreover, by using streptavidin conjugated to Alexa Fluor 488 to detect exogenous biotin, we observed a strong signal (Figure S6A) demonstrating that GNL3-BirA-FLAG is well localized and can biotinylate proteins in its proximity. In four independent experiments, we induced expression of GNL3-BirA-FLAG with DOX for 16 hours and labelled proteins in its proximity with exogenous biotin for 4 hours. Then we purified the biotinylated proteins on streptavidin beads and analyzed them by mass spectrometry. We calculated the LogRatio of the peptides detected upon addition of DOX and biotin compared to the peptides detected in the negative controls (treatment with either DOX or biotin alone) and represented the data in a Volcano plot (Figure 6A). As expected, GNL3 was highly enriched as well as several nucleolar proteins that are known to be in proximity (e.g., GNL3L, GNL2, DDX21, Ki67 or NPM1). Notably, enrichment of ORC2, one of the components of the origin recognition complex, suggested a possible mechanism in the regulation of replication origin firing by GNL3. To confirm the association of ORC2 with GNL3, we immunoprecipitated each of the proteins and analyzed the immunoprecipitates by western blotting; we found GNL3 in immunoprecipitates of ORC2 and *vice versa* (Figure 6B). Mass spectrometry analysis of the proteins that co-immunoprecipitated when using a specific antibody against ORC2 confirmed the presence of GNL3 and most of the ORC subunits, whereas immunoprecipitation with an irrelevant control IgG contained neither GNL3 nor ORC subunits. Moreover, there was a significant overlap between the co-immunoprecipitated proteins and those found by BioID of GNL3: among the 88 proteins significantly enriched by BioID, 35 were found by coimmunoprecipitation with ORC2 (Figure S6B) and most of them (24/35) are proteins localized in the nucleolus. This suggests that at least a subset of ORC2 might be localized in the nucleolus and that the interaction between ORC2 and GNL3 is likely to occur in this compartment. The association of GNL3 with chromatin (Figure 2C), however, suggests that GNL3 and ORC2 also interact at or near replication origins. To test this, we performed GNL3 chromatin immunoprecipitation followed by deep sequencing (ChIP-seq) and found 3412 binding sites for GNL3. We compared these binding sites with ORC2-binding sites (Miotto et al., 2016) but found no significant

overlap (Figure 6C, Figure S6C), indicating that the GNL3–ORC2 interaction occurs in the nucleolus rather than on vicinity of replication origins. To confirm this, we analyzed the GNL3-ORC2 interaction by using PLA and found most foci at the border of regions that stained lightly with DAPI and that correspond to nucleoli (Figure 6D), thus supporting our hypothesis. The PLA signal was strongly decreased upon depletion of GNL3, validating its specificity. Altogether, our data prove that GNL3 and ORC2 interact in the nucleolus suggesting a possible mechanism to regulate replication origins firing and limit DNA resection.

GNL3 regulates ORC2 sub-nuclear localization

ORC2 play roles independently of its function in the ORC complex, possibly at centromeres (Prasanth et al., 2004; Shimada and Gasser, 2007), that are often localized in the vicinity of the nucleolus (Padeken et al., 2013; Wong et al., 2007). In support to this, we observed an interaction between GNL3 and the centromere-specific histone H3 variant CENP-A using PLA (Figure S7A, S7B). We therefore asked whether ORC2 recruitment at centromeres depends on GNL3 by performing PLA between ORC2 and CENP-A. As expected, many PLA foci of ORC2 and CENP-A were found in normal cells when compared to controls treated with only the antibody against ORC2 or that against CENP-A. When the cells were depleted of GNL3, however, the average number of PLA foci per cell was reduced by about two-fold (Figure 7A and 7B), indicating that ORC2 recruitment at centromeres depends in part on the availability of GNL3. Since ORC2 is required to maintain heterochromatin at centromeres (Huang et al., 2016), we tested the impact of GNL3 depletion on centromeric heterochromatin by analyzing the proximity of H3K9me3 and CENP-A by PLA. We found that GNL3 depletion increases the proximity, suggesting that GNL3 may regulate ORC2 centromeric functions (Figure S7C, S7D). We conclude that the presence of ORC2 at centromeres may reflect its nucleolar localization and could be regulated by GNL3 suggesting that GNL3 may regulate ORC2 sub-nuclear localization.

Accumulation of GNL3 in the nucleolus limits DNA resection in response to replicative stress, we then asked if it was related with the regulation of ORC2 sub-nuclear localization by GNL3. To test this, we analyzed the interaction of each GNL3 mutant with ORC2 using PLA. We found, as expected, that GNL3-WT, GNL3-dC, GNL3-dI and GNL3-dA interact with ORC2 in the nucleolus (Figure 7C, Figure S7E). In contrast, we observed that GNL3-dB, and GNL3-dG to a less extent (Figure S7E), interacts with ORC2 mostly in the nucleoplasm (Figure 7C, Figure S7F) consistent with its localization (Figure S7G). One possibility may be that the fraction of GNL3-dB localized in the nucleoplasm interacts with ORC2 on chromatin. If this is true GNL3-dB should be recruited onto chromatin like endogenous GNL3 (Figure 2C).

We found that both GNL3-WT and GNL3-dB were localized on chromatin (Figure 7D), however, we noticed that GNL3-dB, but not GNL3-WT, was also really abundant in the soluble fraction. GNL3-WT and GNL3-dB are localized to the nucleolus but only GNL3-dB diffuses in the nucleoplasm. We hypothesized that GNL3-dB present in the soluble fraction may be nucleoplasmic. To test this, we performed immunofluorescence experiment in presence of cytoskeletal (CSK) to remove soluble proteins. Strikingly, we observed that the signal corresponding to GNL3-dB in the nucleoplasm was strongly reduced (Figure 7E). We conclude that when GNL3-dB is localized in the nucleoplasm it is not associated with chromatin. Since ORC2 is mainly associated with chromatin (Ohta et al., 2003), we postulate that GNL3-dB interacts with a fraction of ORC2 that may be released from the nucleolus. This is consistent with the strong decrease of nucleolar ORC2-GNL3-dB PLA signal (Figure 7D). We propose that the inability of GNL3-dB to accumulate in the nucleolus may lead to the release of ORC2 from the nucleoplasm. This may explain why GNL3-dB is defective for nascent strand protection since it cannot properly regulate ORC2 sub-nuclear localization in order to limit replication origins firing.

Discussion

GNL3/nucleostemin was discovered twenty years ago as a nucleolar protein required for cell proliferation (Tsai and McKay, 2002) and several studies have highlighted its role(s) in maintaining genome integrity (Tsai, 2014). Here, we investigate the role of GNL3 during DNA replication. We demonstrate that GNL3 is a new replisome component that limits origin firing and interacts with ORC2. During replication stress, GNL3 protects the DNA at stalled replication forks from resection by endonucleases and this protection depends on the number of replication origins that fire. We propose a model in which GNL3 is required for accurate DNA replication by controlling origin firing through the regulation of ORC2 sub-nuclear localization (Figure 7F).

GNL3 limits origin firing

We show that GNL3 is new replisome component. However, quantification of iPOND-MS data indicates that GNL3 is not as abundant as the canonical components of replication forks (Ribeyre et al., 2021), suggesting that it may not be associated with every replication fork. GNL3 may be associated with forks in regions of heterochromatin, as, for example, in FANCJ-knockout cells in which GNL3 was found on nascent DNA (Peng et al., 2018; Schwab et al., 2013). The localization of GNL3 in the nucleolus also suggests it may be associated mostly with nascent DNA within heterochromatin since nucleolar associated domains (NADs) are enriched in heterochromatin (Bersaglieri et al., 2022). The association of GNL3 with at least a subset of replication forks might explain why its depletion leads to stalling of S phase, G2-M arrest and γH2A.X phosphorylation (Lin et al., 2014), as well as the increased frequency of MiDAS that we observed. Upon GNL3 loss, replication fork speed slows, suggesting GNL3 might act as fork accelerator, as does PRIMPOL (Bianchi et al., 2013; Schiavone et al., 2016). The fact that GNL3 depletion has no effect on the slowing of fork velocity by CPT, however, argues against this hypothesis. When GNL3 is depleted many origins fire, indicating that GNL3 is an inhibitor of origins firing. We propose that slow replication fork speed observed upon GNL3 depletion is a compensation mechanism for the increased replication origin firing (Ge et al., 2007; Ibarra et al., 2008) rather than a direct impact of GNL3 depletion on replication forks speed. The abundance of GNL3 in the nucleolus as well as its interaction with ORC2 (see below) strongly support this model. The consequences of GNL3 depletion on S-phase are likely to be a consequence of impaired origin firing regulation. Surprisingly, despite the role of GNL3 in the regulation of origins firing, we saw no impact of GNL3 depletion on global replication timing. How might we explain

this apparent discrepancy? The measurement of replication timing is an average of thousands of cells and does not represent stochastic variations between individual cells. Recent data suggest that the firing of replication origins is more stochastic than previously thought (Klein et al., 2021; Wang et al., 2021). GNL3 depletion may, therefore, increase the firing of specific origins without impacting replication timing globally.

GNL3 protects stalled replication forks from resection by limiting replication origins firing

GNL3 protects nascent DNA at stalled replication forks from resection by endonucleases. The increased resection seen upon GNL3 depletion, we conclude, is related to the increased replication origin firing because it is suppressed by an inhibitor of CDC7 that decreases origin firing. This conclusion is consistent with data showing that CDC7 inhibition prevents nascent strand resection (Jones et al., 2021; Sasi et al., 2018). We propose that the replication stress induced by HU in GNL3-depleted cells is exacerbated since a proper control of firing is required (inactivation of late origins and activation of dormant origins), thus leading to DNA resection and replisome collapse. Consistent with this, we found that inhibition of ATR or WEE1, both of which increase origin firing, increases the resection of nascent DNA in a CDC7-dependent manner. Also, inhibition of ATR or WEE1 increases DNA lesions upon exposure to HU due to the exhaustion of the RPA pool (Toledo et al., 2013) and confirms that incorrect control of origin firing leads to DNA resection.

The nascent DNA resection that occurs in the absence of BRCA1 was not suppressed by CDC7 inhibition. This indicates a direct role for BRCA1 in protecting nascent DNA but not in origin firing. Thus, we conclude that nascent DNA resection can be promoted either by loss of a protein that protects the DNA directly, like BRCA1, or by loss of proteins such as GNL3 and WEE1 that are not recruited to nascent DNA and therefore must act indirectly. BRCA1, FANCD2 and RAD51 were the first proteins found to act as fork protectors (Hashimoto et al., 2010; Schlacher et al., 2011; Schlacher et al., 2012) by being recruited to nascent DNA (Dungrawala et al., 2015; Lossaint et al., 2013). Since then, several other proteins have been found to protect stalled forks from resection by nucleases (Berti et al., 2020; Liao et al., 2018; Rickman and Smogorzewska, 2019). Given our findings here, it would be interesting to investigate whether these proteins protect replication forks directly or indirectly.

GNL3 regulates ORC2 sub-nuclear localization

To understand how GNL3 prevents DNA resection, we expressed a series of GNL3 truncations (Tsai and McKay, 2002, 2005). We conclude that the accumulation of GNL3 in the nucleolus prevents DNA resection

is response to replicative stress. One of the main features of GNL3 is its strong residency time in the nucleolus (Meng et al., 2007), this ability may allow GNL3 to sequester specific proteins such as ORC2. Interestingly, GNL3-dB, a mutant that has a lower residency time in the nucleolus (Meng et al., 2006), interacts with ORC2 mostly in the nucleoplasm. GNL3-dB may interact with ORC2 from ORC complex, however since GNL3-dB is not associated with chromatin in the nucleoplasm we do not favor this possibility. We rather think that the interaction between ORC2 and GNL3-dB in the nucleoplasm is due to the release of ORC2 from the nucleolus. We propose that GNL3 may sequester ORC2 to regulate origins firing, this may explain why both GNL3 depletion and expression of GNL3-dB leads to nascent strand resection, since in both cases ORC2 may not be well properly sequestrated in the nucleolus.

Loss of ORC2 increases inter-origin distance (Shibata et al., 2016), therefore GNL3 level in the nucleolus may directly controls ORC2 amount in the nucleoplasm to regulates the number of fired origins. Alternatively, GNL3 may sequester ORC2 in the nucleolus to regulate some of its functions that are not directly linked with the ORC complex such as its role at centromeres (Bauwens et al., 2021; Huang et al., 2016; Prasanth et al., 2004) or in sister chromatid cohesion (MacAlpine et al., 2010; Shimada and Gasser, 2007). In support to this, we found that GNL3 depletion decreases ORC2 recruitment to centromeres and deregulates heterochromatin formation. This is consistent with the possible role of GNL3 in heterochromatin regulation (Maida et al., 2014) and its recruitment to mitotic chromosomes (Oktar et al., 2011) and centromeres (Figure S7A, S7B). In conclusion, the sequestration of ORC2 by GNL3 may regulate the number of origins by affecting their stability but it may also impact ORC2 functions that are not directly related with the ORC complex.

Toward a global role of GNL3 in genome organization

Although GNL3 is found only in chordates, it belongs to the family of YlqF-related GTPases that is conserved in Eukarya, Bacteria and Archea (Mier et al., 2017; Quiroga-Artigas et al., 2022; Reynaud et al., 2005). GNL3 is the more recent member of the family and seemed to have co-evolved with sub compartments of the nucleolus. Growing evidence indicates that the nucleolus is involved in the 3D organization of the genome (Iarovaia et al., 2019) and particularly of centromeric DNA and heterochromatin (Bersaglieri et al., 2022; Padeken et al., 2013; Wong et al., 2007). Therefore, GNL3 may play a larger role in the organization of centromeres, or other regions of heterochromatin, by keeping them in proximity to the nucleolus thanks to its long residency time (Meng et al., 2006). For example, GNL3 may mediate interactions between nucleolus and heterochromatin as proposed for MKI67 (Sobecki et al., 2016) and NPM1 (Holmberg Olausson et al., 2014), two proteins localized to the nucleolar rim like

GNL3 (Stenstrom et al., 2020). It has been recently shown that genome organization is a determinant of the locations of replication origins (Emerson et al., 2022), therefore GNL3 may have a broader in the regulation of replication origins.

Acknowledgments

We thank all the present and former lab members for comments and suggestions on the project and the manuscript. We are grateful to Pierre-Henry Gaillard, Jean-Hugues Guervilly, Maud de Dieuleveult, Anne-Claude Gingras, Yea-Lih Lin and Montpellier Genomic Collection for reagents. We thank Armelle Lengronne, Antoine Aze, Eric Julien, Sébastien Britton, Olivier Ganier and Joelle Nassar for discussions and comments as well as Marie-Pierre Blanchard and Amélie Sarazzin from the Montpellier Imaging Platform for their support. We acknowledge Carol Featherstone of Plume Scientific Communication Services for professional scientific editing during the preparation of the manuscript. We are grateful to Montpellier Combing Facility (Etienne Schwob and Marjorie Drac) and Montpellier GenomiX facility (Hugues Paranello). Mass spectrometry experiments were carried out using the facilities of the Montpellier Proteomics Platform (PPM, BioCampus). We thank Céline Gongora, Nadia Vie and Naoill Abdellaoui for their help with the use of the Celligo. We thank the 3P5 proteom'IC facility (Johanna Bruce, Cedric Broussard and François Guillonneau) at Institut Cochin, which is supported by the DIM Thérapie Génique Région Ile-de-France, IBiSA, and the Labex GR-Ex. This work was supported by a *Jeunes Chercheurs Jeunes Chercheuses* grant from the *Agence National de la Recherche* (REPLIBLOCK ANR-17-CE12-0034-01), and an Emergence grant from *Cancéropole Grand Sud-Ouest* to Cyril Ribeyre as well as a grant from *Programme labellisé Fondation ARC* to Angelos Constantinou. Rana Lebdy was funded by fellowships from Azm & Saade Association and *Fondation ARC pour la recherche sur le cancer*. Benoit Miotto and Anne Letessier are partners of Labex 'Who am I?' (ANR-11-LABX-0071 and ANR-11-IDEX-005-02) and are supported by *Fondation pour la Recherche Medicale* (AJE20151234749), INSERM, CNRS and University Paris Cité. Jean-Charles Cadoret thanks the IdEx Université Paris Cité (ANR-18-IDEX-0001), and the generous legacy from Ms. Suzanne Larzat.

Author contributions

Conceptualization, R.L. and C.R.; Methodology R.L., M.C., J.P, J.A, A.L., J-C.C. and C.R.; Validation R.L. and C.R.; Formal Analysis R.L. J-C.C. and C.R. Funding Acquisition R.L., A.C., R.A M. and C.R. Supervision R.A M. and C.R., Investigation R.L., M.C., J-C.C., A.L. and C.R.; Visualization R.L; Writing – Original Draft R.L. and C.R.; Writing – Review & Editing R.L., J-C.C., A.L., B.M, J.B., A.C, R. A N. and C.R. Data Curation R.L., M.C., J-C.C., A.L. and C.R.

Declaration of interests

The authors declare no competing interests.

Figures Legends

Figure 1. GNL3 is a new replisome component. A. Experimental set-up of iPOND-MS experiment. HeLa S3 cells were pulse-labelled with EdU and chased with thymidine for 2 hrs. **B.** Bar plot showing the LogRatio (pulse/chase) of average peptides intensities corresponding to the indicated proteins from (Ribeyre et al., 2021). Pulse experiments have been repeated 6 times and chase experiments 4 times. **C.** iPOND experiment analyzed by western-blot. HeLa S3 cells were pulsed for 15 min with EdU and chased for 2 hrs with thymidine. In no click sample, biotin-TEG azide was replaced by DMSO. **D.** Western-blot analysis of HeLa S3 cells depleted with a pool of 4 siRNA targeting GNL3 (siGNL3) or not (siControl). **E.** PLA (proximity ligation assay) analyzing the proximity between EdU (coupled with biotin-TEG azide) and GNL3 in HeLa S3 cells. **F.** PLA (proximity ligation assay) analyzing the proximity between EdU (coupled or not with biotin-TEG azide) and GNL3 in HeLa S3 cells.

Figure 2. GNL3 depletion increases firing of replication origins. A. Flow cytometry experiment of HeLa S3 cells. Nascent DNA was labelled with IdU and total DNA stained with propidium iodide. **B.** Quantification of the intensity of IdU signal from flow cytometry analysis. For statistical analysis Mann-Whitney test was used; ****$p<0.0001$. **C.** Western-blot analysis of the indicated proteins upon chromatin fractionation. **D.** Quantification of chromatin fractionation based on 3 independent experiments. **E.** DNA combing experiment. HeLa S3 cells were subjected to two consecutive 20 min pulses of IdU and CldU and analyzed by DNA combing. A representative microscopy image of combed DNA molecules containing IdU (red) and CldU (green) tracks in presented with arrows indicating the direction of replication. **F.** Analysis of replication forks velocity by DNA combing. For statistical analysis Mann-Whitney test was used; ****$p<0.0001$. **G.** Analysis of GIFD (Global Instant Fork Density) by DNA combing in HeLa S3 cells. For statistical analysis paired t-test was used; *$p<0.05$. **H.** Replication timing experiment. HeLa S3 cells were pulse-labelled with BrdU for 90 min and sorted by flow cytometry in two fractions, S1 and S2, corresponding to early and late S-phase. Neo-synthesized DNA was immunoprecipitated with BrdU antibodies. Early and late neo-synthesized DNAs were labeled with Cy3 and Cy5 and hybridized on microarrays. After analyzing with the START-R software, replication-timing profiles can be obtained from two replicates. Shown are the zoomed microarray profiles of the timing of replication on chromosome 1 and chromosome 15 as example. Blue lines represent replication timing from siControl cells and red lines represent siGNL3 cells and grey spots represent the log ratio intensity for each probes of the microarray. Any significantly disturbed regions are detected by START-R software.

Figure 3. GNL3 prevents DNA resection at stalled replication forks. **A.** HeLa S3 cells were sequentially labelled for 30 min with IdU and for 30 min with CldU with or without 1 μM CPT. Ratios between CldU and IdU are plotted, the red line indicates the median. For statistical analysis Mann-Whitney test was used; ****p<0.0001. ns, not significant. **B.** Western-blot analysis of HeLa S3 cells treated with 5 mM HU during the indicated time. **C.** HeLa cells were sequentially labelled for 30 min with IdU and for 30 min with CldU then treated with 5 mM HU for 240 min. The ratio between CldU and IdU is plotted, the red line indicates the median. For statistical analysis Mann-Whitney test was used; ****p<0.0001. **D.** HeLa S3 were sequentially labelled for 30 min with IdU and for 30 min with CldU then treated with 5 mM HU for 240 min. The ratio between CldU and IdU is plotted, the red line indicates the median. For statistical analysis Mann-Whitney test was used; ****p<0.0001. **E.** Western-blot analysis of Flp-in T-Rex HeLa cells expressing GNL3-FLAG. Cells were first transfected with siControl or siGNL3 for 48 hrs then expression of GNL3-FLAG (resistant to the siRNA against GNL3) was induced using 10 μg/ml of doxycycline (DOX) for 16 hrs. **F.** Flp-in T-Rex HeLa cells were sequentially labelled for 30 min with IdU and for 30 min with CldU then treated with 5 mM HU for 240 min. The ratio between CldU and IdU is plotted, the red line indicates the median. For statistical analysis Mann-Whitney test was used; ****p<0.0001.

Figure 4. Resection in the absence of GNL3 is a consequence of its role in origin firing. A. Experimental set-up of iPOND experiment. **B.** iPOND experiment analyzed by Western-blot. Cells were pulsed with 15 min EdU and chased for 2 hrs with 10 μM thymidine or 5 mM HU. In no click sample, biotin-TEG azide was replaced by DMSO. **C.** Scheme to explain how CDC7 inhibition is affecting forks stability. **D.** HeLa S3 were sequentially labelled for 30 min with IdU and for 30 min with CldU then treated with 5 mM HU for 240 min with or without 10 μM of CDC7 inhibitor PHA-767491. The ratio between CldU and IdU is plotted, the red line indicates the median. For statistical analysis Mann-Whitney test was used; ****p<0.0001. **E.** Western-blot analysis of the indicated proteins upon treatment with 5 mM HU for 240 min with or without 10 μM of CDC7 inhibitor PHA-767491. **F.** HeLa S3 cells were sequentially labelled for 30 min with IdU and for 30 min with CldU then treated with 5 mM HU for 240 min with or without 10 μM of CDC7 inhibitor PHA- 767491. The ratio between CldU and IdU is plotted, the red line indicates the median. For statistical analysis Mann-Whitney test was used; ****p<0.0001. ns, not significant. **G.** Cells were sequentially labelled for 30 min with IdU and for 30 min with CldU then treated or not with 5 mM HU for 240 min with or without 10 μM of ATR VE-821 inhibitor or 500 nM of WEE1 inhibitor AZD1775. **H.** The ratio between CldU and IdU is plotted, the red line indicates the median. For statistical analysis Mann-Whitney test was

used; ****p<0.0001. **I.** The ratio between CldU and IdU is plotted, the red line indicates the median. For statistical analysis Mann-Whitney test was used; ****p<0.0001.

Figure 5. Nucleolar accumulation of GNL3 prevents resection. A. Schematic representation of human GNL3 protein with its associated domains (B: basic domain; C: coiled-coil domain; G1: GTP-binding motif 1; G4: GTP-binding motif 4; I: intermediate domain; A: acidic domain). GNL3-WT and GNL3 mutants (dB, dC, dG, DI and dA) are fused with FLAG and are stably inserted in HeLa Flp-In T-Rex cell-line. **B.** Western-blot analysis of Flp-In T-Rex HeLa cells expressing exogenous GNL3-WT or GNL3 mutants. Cells were transfected with siControl or siGNL3 for 48 hrs then expression of exogenous GNL3-FLAG (resistant to the siRNA against GNL3) was induced using 10 μg/ml of doxycycline for 16 hrs. **C.** Immunofluorescence analysis of Flp-in T-Rex HeLa cells expressing exogenous GNL3-WT or GNL3 mutants. **D.** Flp-in T-Rex HeLa cells were sequentially labelled for 30 min with IdU and for 30 min with CldU then treated with 5 mM HU for 240 min. The ratio between CldU and IdU is plotted, the red line indicates the median. For statistical analysis Mann-Whitney test was used; ****p<0.0001; ***p<0.001; **p<0.01; ns non significant.

Figure 6. GNL3 interacts with ORC2 in the nucleolus. A. GNL3-BioID experiment analyzed by mass spectrometry. Expression of GNL3-BirA-FLAG in HEK293 Flp-in cells was induced with doxycycline for 16 hrs then biotin was added for 4 hrs. For negative controls cells were treated either 16 hrs with doxycycline either 4 hrs with biotin. Each condition was performed four times and analyzed by mass spectrometry. Label free quantification was performed using MaxQuant (Cox and Mann, 2008) and statistical analysis using Perseus (Tyanova et al., 2016). The volcano plot shows the proteins that are significantly enriched upon induction of GNL3-BirA-FLAG and addition of biotin. **B.** Western-blot analysis of GNL3 and ORC2 immunoprecipitates in K562 cells. **C.** Comparison of the genomic location of GNL3 and ORC2. Chromatin immunoprecipitation of GNL3 followed by deep sequencing was performed in HeLa S3. GNL3 binding sites were compared to ORC2 binding sites obtained from Miotto et al. (Miotto et al., 2016). **D.** PLA (proximity ligation assay) analyzing the proximity between ORC2 and GNL3 in HeLa S3 cells.

Figure 7. GNL3 regulates ORC2 sub-nuclear localization. A. PLA (proximity ligation assay) analyzing the proximity between ORC2 and CENP-A in HeLa S3 cells using the indicated antibodies. **B.** Graphic representation of the average number of PLA ORC2-CENP-A foci. The error bars represent the variation between 3 independent experiments. **C.** PLA (proximity ligation assay) analyzing the proximity between ORC2 and GNL3-FLAG or GNL3-dB-FLAG, in HeLa Flp-In cells upon doxycycline induction. **D.** Western-blot analysis of the indicated proteins upon chromatin fractionation in HeLa Flp-In cells expressing either GNL3-WT or GNL3-dB. **E.** Immunofluorescence experiment HeLa Flp-In cells expressing GNL3-dB with or

without pre-extraction with cytoskeletal buffer (CSK). **F.** GNL3 is localized mainly in the nucleolus in proximity of nascent DNA and sequesters ORC2 to regulate the number of replication origins by possibly keeping it at vicinity of centromeres and heterochromatin. In absence of GNL3, ORC2 is no longer sequestrated and an excessive number of replication origins may be fired.

Methods

Cell lines

HeLa S3 (obtained from ATCC), Flp-In T-Rex 293 (obtained from ThermoFisher) and HeLa Flp-In T-Rex (authenticated with Eurofins, gift from Jean-Hugues Guervilly and Pierre-Henri Gaillard, Centre de Recherche en Cancérologie de Marseille, France) cells were cultured in Dulbecco's modified Eagle's media (DMEM). HCT116 (obtained from SIRIC Montpellier Cancer) and K562 (authenticated with Eurofins) cells were cultured in Roswell Park Memorial Institute medium (RPMI). Culture media was supplemented with 10% fetal bovine serum (Biowest) and penicillin/streptomycin (Sigma-Aldrich). Cells were incubated in a 5% CO_2 at 37°C. Selection of integrated clones in Flp-In cells were done using hygromycin and blasticidin.

Inhibitors, drugs and antibiotics

The following reagents were used: etoposide (Sigma-Aldrich E1383), camptothecin (Sigma-Aldrich C9911), hydroxyurea (Sigma-Aldrich H8627), doxycycline (Clontech 631311), hygromycin B Gold (InvioGen), zeocin (Invitrogen 46-0509), blasticidin (InvivoGen), ATR inhibitor VE-821 (TINIB-TOOLS), WEE1 inhibitor AZD1775 (Selleckchem), CDC7 inhibitor PHA-767491 (Selleckchem).

Plasmids construction

GNL3 cDNA cloned in pDONR223 (obtained from Montpellier Genomic Collection) was introduced using Gateway method in pDEST-pcDNA5-FLAG C-term and pDEST-pcDNA5-BirA-FLAG C-term (gifts from Anne-Claude Gingras, Lunenfeld-Tanenbaum Research Institute at Mount Sinai Hospital, Toronto, Canada). GNL3 truncations were created by gene synthesis (Invitrogen GeneArt Gene Synthesis) and introduced using Gateway method into pDEST-pcDNA5-FLAG C-term.

Gene silencing

For GNL3 depletion siGENOME SMARTpool (M-016319-00) and individual siRNA oligonucleotide (D-016319-01-0002) were purchased from Dharmacon and transfected using INTERFERin (Polypus transfection). siRNAs against MRE11 and CtIP were provided by Yea-Li Lin (Institut de Génétique Humaine, Montpellier) and are described in (Coquel et al., 2018).

Western-blot

Cellular extracts were resuspended in Laemmli buffer (65.8 mM Tris, 26.3% glycerol, 2.1% SDS, and Bromophenol blue) and boiled at 95°C for 5 min. Proteins were separated by SDS-PAGE using home-made

or precast gels (Bio-Rad) with suitable percentage then transferred on nitrocellulose membranes (GE Healthcare or Bio-Rad). Membranes were blocked with 5% non-fat milk in TBS-T (10 mM Tris pH 8.0, 150 mM NaCl, 0.5% Tween 20) for 1 hr then incubated with the primary antibodies overnight. Membranes were washed 3 times with TBS-T then incubated with the corresponding secondary antibody. Finally, membranes were developed with Clarity Western ECL Blotting Substrate (Bio-Rad) and images were acquired using a ChemiDoc System (Bio-Rad). Antibodies against the following proteins were used: Ser345 Phospho-Chk1 (Cell Signaling Technology 2348), Chk1 (Santa Cruz sc-8408), PCNA (Sigma-Aldrich P8825), Ser4/8 Phospho-RPA32 (Bethyl A300-245A), RPA32 (Calbiochem NA18), histone H3 (Abcam ab62642), GNL3 (Bethyl A300-600A, Santa Cruz sc-166460 or Sigma-Aldrich SAB1407312), Ser33 Phospho-RPA32 (Bethyl A300-246), Tubulin (Sigma Aldrich T5168), CDC45 (Santa Cruz sc-20685), Ser40 Phospho-MCM2 (Abcam ab133243), MRE11 (Novus NB100-142), BRCA1 (Santacruz sc-642), CtIP (Abcam ab70163), RAD51 (Santa Cruz sc-8349) and FLAG (Sigma Aldrich F1804).

esiRNA screening

The 25 esiRNA (Sigma-Aldrich) corresponding to 24 candidates plus 1 negative control (EGFP) are described in SupTable1. HCT116 were seeded in 96 wells plates and transfected with esiRNAs using Oligofectamine (ThermoFisher). After 48 hours, transfected cells were subjected to 4 hrs treatment with 1 μM camptothecin then fixed for 15 min using 4% paraformaldehyde (PFA). Cells were permeabilized with 75% EtOH for 30 min on ice. 96 wells plate was incubated with primary antibody against Ser139 Phospho-H2A.X (Millipore 05-636) for 60 min then with secondary antibody anti-mouse coupled with Alexa568 (ThermoFisher A-11011) and finally with DAPI for 30 min. All the washes were performed with PBS-BSA 1%. 96 wells were scanned using a Nexcelom Celigo and images were analyzed using Celigo software. DAPI staining was used to measure the level of Ser139 Phospho-H2A.X in the nucleus for each esiRNA.

Proximity Ligation Assay (PLA)

Cells were grown on coverslips to reach 70-80% confluency then fixed with 2% paraformaldehyde (PFA) and 0.02% sucrose in PBS for 20 min at room temperature. When specified cells were incubated with EdU (5-ethynyl-2'-deoxyuridine) for the indicated times. Cells were permeabilized with 0.5% Triton X100- PBS for 20 min then washed PBS-3% BSA. EdU was conjugated to biotin-TEG-azide (Eurogentec) using Click-it reaction (30 min at room temperature) using indicated concentrations (10 mM sodium Ascorbate, 5 μM biotin-TEG-azide, 3 μM $CuSO_4$). For Click-it negative controls, biotin-TEG-azide was replaced by DMSO.

Coverslips were incubated with primary antibodies in PLA blocking solution (Sigma-Aldrich) overnight at 4°C then washed with PBS. PLA probes (anti-mouse minus DUO92004 and anti-rabbit plus DUO92002, Sigma-Aldrich) were incubated together in PLA blocking solution for 20 min then added on the coverslips for 1 h at 37°C then washed 2 times with buffer A (150 mM NaCl, 10 mM Tris, 0.5 % Tween). PLA kit was used (DUO92014, Sigma-Aldrich) for the following steps. Coverslips were incubated with ligase (1/40 dilution in ligase buffer) for 30 min at 37°C. Coverslips were washed 2 times with buffer A and incubated with polymerase (1/80 dilution in amplification buffer) for 100 min at 37°C. Coverslips were washed 2 times with buffer B (200 mM NaCl, 400 mM Tris-Base), dried and then mounted on glass slides with DAPI containing mounting medium (DUO82040 Sigma-Aldrich). Cells were analyzed by fluorescence microscopy and quantification the number of foci was performed using Fiji software. Antibodies against the following proteins were used: Biotin (Bethyl A150-109 and Jackson Immunoresearch 200-002-211), ORC2 (Bethyl A302-734A), CENP-A (Thermo Fisher MA1-20832), FLAG (Sigma Aldrich F1804), H3K9me3 (Abcam ab8898) and GNL3 (Bethyl A300-600A and Santa Cruz sc-166460).

Flow Cytometry

When indicated cells were first labeled with 20 µM IdU for 10 min and then fixed with ice-cold 70% ethanol. Then cells were treated with RNase during 60 min and then for 30 minutes with 2M HCl. Next, the cells were incubated with a BrdU/IdU antibody from BD Biosciences (347580) for 60 min or with an anti-pH3S10 (Cell Signaling 9701) overnight, and then with an Alexa 488 conjugated anti-mouse IgG (Invitrogen) at room temperature for 30 min. Finally, the cells were stained with 5 µg/ml of propidium iodide in PBS and analyzed using a MACSquant analyzer (Miltenyi Biotec). Results were analyzed using Flowjo (https://www.flowjo.com).

Replication analysis by DNA Combing

Asynchronous cells were labeled 20 min with IdU, 20 min with CldU and then chased 90 min with thymidine. Purification of HMW gDNA, DNA combing and replication analysis was performed as in (Bialic et al., 2015) with the following modifications. Agarose plugs containing gDNA were washed in TNE50 containing 100 mM NaCl, digested O/N at 42°C with 3U β-agarase (New England Biolabs) and again for 2 hrs with 2U β-agarase. DNA was combed in MES buffer also containing 100 mM NaCl. Briefly, genomic DNA was combed on silanized coverslips, denatured with NaOH, and sites of DNA synthesis revealed using anti-IdU (red), anti-CldU (green), and anti-ssDNA (blue) antibody pairs. Primary antibodies were rat anti-BrdU (clone BU1/75, Abcam ab6326) for CldU, mouse anti-BrdU (clone B44, Becton Dickinson), for IdU

and mouse autoanti-ssDNA (from DSHB) for DNA. Washes were performed with PBS-T containing 0.05% Triton X100. Secondary antibodies were Alexa488 Goat anti-rat IgG, Alexa546 Goat anti-mouse IgG, Alexa647 Goat anti-Mouse IgG2a (Life Technologies). Imaging was performed on a Zeiss AxioImager Z1 microscope with YFP, Cy3 and Cy5 filter blocks, equipped with a 40× objective (EC Plan Neofluar 1.3 NA oil) and scMOS ZYLA 4.2 MP camera (2048*2048 pixels, 6.5µm pixel size). Red-to-green signals show fork direction (yellow arrow). Fork velocity (FV) is calculated by dividing the length of the green tract by the pulse time (in kb/min). Global instant fork density (GIFD) was calculated using the formula that accounts for the doubling of DNA during S phase:

$$GIFD = \frac{Nf/DNA \times (G1\% \times 0.66) + S\% + (G2M\% \times 1.33)}{S\%}$$

where Nf is the number of bicolor forks, DNA the total length of DNA measured (in Mb) and G1%, S% and G2M% the fraction of cells in G1, S and G2 or M phases, respectively, calculated from flow cytometry profiles using the same cells as for DNA combing.

Isolation of proteins on Nascent DNA (iPOND)

iPOND was performed largely as previously described (Lossaint et al., 2013; Ribeyre et al., 2016). HeLa S3 cells were pulse labeled with 10 µM EdU for indicated times and chases were performed with 10 µM thymidine. Cells were fixed with 1% formaldehyde for 5 min or 2% for 15 min followed or not by quenching of formaldehyde by 5 min incubation with 0.125 M glycine. Fixed samples were collected by centrifugation at 1000 g for 3 min, washed three times with PBS and stored at -80°C. Cells were permeabilized with 0.5% triton for 30 min and click chemistry was used to conjugate biotin-TEG-azide (Eurogentec) to EdU-labelled DNA in PBS containing 10 mM sodium Ascorbate, 10 µM biotin-TEG-azide, 2 mM $CuSO_4$. Cells were re-suspended in lysis buffer (10 mM Hepes-NaOH; 100 mM NaCl; 2 mM EDTA PH8; 1 mM EGTA; 1 mM PMSF; 0.2% SDS; 0.1% Sarkozyl) and sonication was performed using a Qsonica sonicator with the following settings: 30% power, 20 sec constant pulse and 50 sec pause for a total sonication time of 5 min on ice with water. Lysates were centrifuged at 15,000 g for 10 min at room temperature. Supernatants were normalized by DNA quantification using a nanodrop device. Biotin conjugated DNA-protein complexes were captured using overnight incubation with magnetic beads coated with streptavidin (Ademtech). Captured complexes were washed with lysis buffer and 500 mM NaCl. Proteins associated with nascent DNA were eluted under reducing conditions by boiling into SDS sample buffer for 30 min at 95°C and analyzed by Western-blot or mass spectrometry as indicated in (Kumbhar et al., 2018). Analysis of raw files was performed using MaxQuant (Cox and Mann, 2008) using default settings with label-free

quantification option enabled. Raw file spectra were searched against the human UniProt reference database. Protein, peptide, and site false discovery rate (FDR) were adjusted to < 0.01.

DNA fibers labelling

DNA fibers labelling was performed as previously described (Lossaint et al., 2013; Ribeyre et al., 2016). Cells were labeled with 25 μM IdU, washed with warm media and exposed to 50 μM CldU. Cells were lysed and DNA fibers were stretched onto glass slides are left to air dry then are fixed in methanol/acetic acid (3:1) for 10 min. The DNA fibers were denatured with 2.5 M HCl for 60 min, washed with PBS and blocked with 2% BSA in PBS-Tween for 60 min. IdU replication tracks were revealed with a mouse anti-BrdU/IdU antibody from BD Biosciences (347580) and CldU tracks with a rat anti-BrdU/CldU antibody from Eurobio (ABC117-7513). The following secondary antibodies were used: Alexa fluor 488 anti-mouse antibody (Life A21241) and Cy3 anti-rat antibody (Jackson Immunoresearch 712-166-153). Fibers were visualized and imaged by Carl Zeiss Axio Imager Apotome using 40X Plan Apo 1.4 NA oil immersion objective. Replication tracks lengths were analyzed using ImageJ software. Statistical analysis was performed using Graphpad Prism software.

Immunofluorescence

Cells were grown on coverslips to reach 70-80% confluency then directly with 4% paraformaldehyde (PFA) in PBS for 20 min at room temperature. When indicated, incubation with cytoskeletal (CSK) buffer (10 mM PIPES pH 6.8, NaCl 100mM, sucrose 300 mM, MgCl2 3mM, EGTA 1mM, Triton X-100 0.5%) was performed. Cells were permeabilized by with 0.2% Triton X100- PBS for 10 min then transferred into 0.1% Tween-PBS for 5 min. Coverslips were then incubated with primary antibodies in 0.1% Tween-5% BSA-PBS for 1-2 hrs, washed with 0.1% Tween-PBS, then incubated with secondary antibodies (anti-mouse or anti-rabbit coupled with Alexa fluor 488 or Alexa Fluor 546) in Tween 0.1%-BSA 5%-PBS for 1 hr. All the incubations were carried out in darkness in a humidified chamber at room temperature. Finally, coverslips are washed again with 0.1% Tween-PBS, incubated with Hoechst to label DNA for 5 min, and then mounted on glass slides with Prolong (Life). Cells were analyzed by fluorescence microscopy. Antibodies against the following proteins were used: FLAG (Sigma Aldrich F1804), Streptavidin-Alexa Fluor 488 (Life S32354) and GNL3 (Bethyl A300-600A).

Replication timing experiments and microarrays

Cells were incubated with 50 μM of BrdU for 90 min and collected, washed three times with PBS and then fixed in ethanol 75%. Cells were re-suspended in PBS with RNAse (0.5 mg/ml) and then with propidium

iodide (50 µg/ml) followed by incubation in the dark at room temperature for 30 min with low agitation. Two fractions of 150,000 cells, S1 and S2 corresponding to Early and Late S-phase fractions respectively, were sorted by flow cytometry using a Becton Dickinson FACS Melody. Whole DNA was extracted with lysis buffer (50 mM Tris pH 8, 10 mM EDTA, 300 mM NaCl, 0.5% SDS) and 0.2 mg/ml of Proteinase K for 2 hrs at 65°C. Neo-synthesized DNA were immunoprecipitated with BrdU antibodies (Anti-BrdU Pure, BD Biosciences, #347580) as previously described (Fernandez-Vidal et al., 2014). To control the quality of enrichment of early and late fractions in S1 and S2, qPCR was performed with BMP1 oligonucleotides (early control) and with Dppa2 oligonucleotides (late control; data not shown, (Hiratani et al., 2008)). Microarray hybridization requires a minimum of 1000 ng of DNA. To obtain sufficient specific immunoprecipitated DNA for this hybridization step, whole genome amplification was conducted (WGA, Sigma) on immunoprecipitated DNA. A post WGA qPCR was performed to preserve specific enrichment in both S1 and S2 fractions. Early and late amplified neo-synthesized DNA were then labeled with Cy3 and Cy5 ULS molecules, respectively (Genomic DNA labeling Kit, Agilent). The hybridization was performed according to the manufacturer instructions on 4×180K mouse microarrays (SurePrint G3 Mouse CGH Microarray Kit, 4x180K, AGILENT Technologies, reference genome: mm9). Microarrays were scanned with an Agilent High-Resolution C Scanner using a resolution of 3 µm and the autofocus option. Feature extraction was performed with the Feature Extraction 9.1 software (Agilent Technologies). For each experiment, the raw data sets were automatically normalized by the Feature extraction software. Analysis was performed using the STAR-R software described in (Hadjadj et al., 2020). The statistical comparison was conducted between early and late domains from both cell lines in order to determine segments where replication timing changes. Graphical representation was generated with START-R suit.

Chromatin immunoprecipitation and deep sequencing (ChIP-seq)

About 20.10^6 of Hela S3 cells per sample were prepared for sonication following the True-ChIP chromatin shearing kit protocol for High Cell concentration from Covaris. Cells were cross-linked in 1% methanol-free formaldehyde during 5 min before cell lysis and nuclei preparation. Washed nuclei were sonicated for 15 min at 6°C to obtain DNA fragments of 100-800pb using the E220evolution Covaris machine following parameters indicated in the provided protocol. After dilution with one volume of immunoprecipitation dilution buffer (Covaris), sonicated samples were pre-cleared with 3 µL/mL of protein G magnetic beads (Ademtech) during 1 hr at 4°C. Each sample was then normalized to an equal amount of protein (associated to pre-cleared chromatin) and input samples were collected after this step. Normalized samples were then incubated with 1 µg of GNL3 antibody (Bethyl A300-600A) overnight at

4°C, before incubation with 20 µL/mL of protein G magnetic beads (previously blocked overnight at 4°C in immunoprecipitation dilution buffer with 1% BSA) during 4 hrs at 4°C. Chromatin bound to beads was then washed 5 min at room temperature in each following buffers: low salt buffer (150 mM NaCl, 20 mM Tris HCl pH=8, 2 mM EDTA, 1% Triton, 0.1% SDS); high salt buffer (500 mM NaCl, 20 mM Tris HCl pH=8, 2 mM EDTA, 1% Triton, 0.1% SDS); LiCl buffer (0.25 M LiCl, 10 mM Tris-HCl pH=8, 1 mM EDTA, 1% Sodium deoxycholate, 1% NP-40); TE buffer (10 mM Tris-HCl pH=8, 1 mM EDTA). Washed beads were eluted in 200 µL of elution buffer (100 mM NaHCO3, 1% SDS) during 15 min at 30°C with shaking. Eluted chromatin and input samples were reverse-crosslinked overnight at 65°C with 0.2 M NaCl and 0.02 mg/mL of RNAse A and incubated 1 hr with Proteinase K (400 µg/mL final concentration). DNA was purified using the ChIP DNA Prep Adem kit (Ademtech) following the provided protocol. DNA bound to beads was eluted in 50 µL of elution buffer. Quantity of DNA was measured with the Qubit 1X dsDNA HS Assay kit (Invitrogen), using a Qubit 2.0 fluorometer (Thermofisher scientific). GNL3 ChIP was repeated three times and 10 ng of each ChIP and each corresponding input were pooled together and send to the MGX sequencing platform of Montpellier, France (https://www.mgx.cnrs.fr/). DNA banks were sequenced using the Illumina-Novaseq-6000 machine to obtain 150 bp paired-end reads. Sequencing data were processed and analyzed using the online Galaxy platform (https://usegalaxy.org/). Reads were aligned on the February 2009 human reference genome (GRCh37/Hg19) using Bowtie2 tool with default parameters. GNL3 Peaks were discovered using MACS2 callpeak tool using input as control file with a q-value<0.005. ORC2 peaks file was taken from Miotto et al. (Miotto et al., 2016).

MiDAS

Cells were seeded on coverslips and synchronized using 2 mM of thymidine for 18 hrs. After the thymidine block cells were washed twice with pre-heated media and released for 8 hrs after which they were labelled with 10 µM EdU for 15 min and collected by direct fixation of 4% PFA into the media to avoid loss of mitotic cells. Cells were then immunostained with anti-pH3S10 (Cell Signaling 9701) and EdU was clicked with Alexa fluor 555 using Click chemistry.

Chromatin Fractionation

Cells were seeded at 80% confluency and collected by trypsinization followed by centrifugation for 3 min (1200g) at room temperature. The pellets were washed with PBS then resuspended with CSK buffer (10 mM PIPES pH 6.8, 100 mM NaCl, 300 mM Sucrose, 1 mM $MgCl_2$, 1 mM EGTA, 0.5 mM DTT, 0.1% Triton X-100, 1 mM ATP, 1X protease inhibitor) and kept for 10 min on ice. Lysed cells were then centrifuged for 3

min (3000g) at 4°C. The resulting supernatant presenting the soluble protein fraction was transferred to another Eppendorf tube and the pellet was washed with CSK buffer for 10 min on ice followed by centrifugation for 3 min (3000g) at 4°C. the resulting pellet which represents the in-soluble fraction of proteins was then resuspended in 2X Laemmli buffer and incubated at 95°C for 10 min before western blot analysis.

Bio-ID

Flp-In T-Rex 293 cell lines were stably transfected with Flag-BirA-GNL3. Cells seeded at 75% confluency were incubated with 10 µg/ml of doxycycline for 16 hrs and then with 50 µM biotin for 4 hrs. Cells were washed once with PBS and lysed with RIPA/SDS buffer (50 mM Tris-HCl pH 7.5, 150 mM NaCl, 1 mM EDTA, 1 mM EGTA, 1% NP-40, 0.2% SDS, 0.5% Sodium deoxycholate) complemented with 1X complete protease inhibitor and 250U benzonase (Sigma-Aldrich, CE1014). Lysed cells were incubated on a rotating wheel for 1 hr at 4°C followed by sonication on ice with 30% amplitude for 3 cycles of 10 sec (2 sec ON-2sec resting) separated with 10 sec of resting. Sonicated lysate was next centrifuged for 30 min (7750g) at 4°C, the cleared supernatant was transferred to a new tube and protein concentration was quantified using Bradford protein assay. For each condition, 500 µg of proteins were incubated with 30 µl of Streptavidin-Agarose beads (Sigma-Aldrich, CS1638) on a rotating wheel for 3 hrs at 4°C. Beads were next washed sequentially with 1 ml of each buffer starting with lysis buffer, wash buffer 1 (2% SDS in H_2O), wash buffer 2 (0.2% sodium deoxycholate, 1% Triton X-100, 500 mM NaCl, 1mM EDTA, and 50mM Hepes pH 7.5), wash buffer 3 (250 mM LiCl, 0.5% NP-40, 0.5% sodium deoxycholate, 1mM EDTA, 500mM NaCl and 10mM Tris pH 8) and finally wash buffer 4 (50 mM Tris pH 7.5 and 50 mM NaCl). Biotinylated proteins were eluted from the magnetic beads using 40 µl of 2X Laemmli buffer and incubated at 95°C for 10 min.

Proteomics analysis of Bio-ID samples

Biotinylated proteins were migrated on SDS PAGE for a short migration. After reduction (DTT 1 M, 30 min at 60°C) an alkylation (IAA 0.5 M, 30 min RT) proteins were digested using trypsin (Gold, Promega, 1ug / sample, overnight at 37°C). For LC MSMS analysis, samples were loaded onto a 50 cm reversed-phase column (75 mm inner diameter; Acclaim PepMap 100 C18; Thermo Fisher Scientific) and separated with an UltiMate 3000 RSLC system (Thermo Fisher Scientific) coupled to a QExactive HF system (Thermo Fisher Scientific). Separation of the peptides was performed following a gradient from 2 to 25% buffer B (0.1% AF in 80% ACN) for 100 min at a flow rate 300 nl / min, then 25 to 40% in 20 min and finally 40 to 90% in 3 minutes. Tandem mass spectrometry analyses were performed in a data-dependent mode. Full scans

(350–1,500 m/z) were acquired in the Orbitrap mass analyzer with a resolution of 60,000 at 200 m/z. For MS scans, 3e6 ions were accumulated within a maximum injection time of 60 ms. The 12 most intense ions with charge states ≥2 were sequentially isolated (1e5) with a maximum injection time of 100 ms and fragmented by higher-energy collisional dissociation (normalized collision energy of 28) and detected in the Orbitrap analyzer at a resolution of 30,000. Raw spectra were processed with MaxQuant v 1.6.5.0 (Cox and Mann, 2008) using standard parameters with match between runs option. Spectra were matched against the UniProt reference proteome (release 2019_06; http://www.uniprot.org) of Homo sapiens and 250 frequently observed contaminants, as well as reversed sequences of all entries. The maximum false discovery rate for peptides and proteins was set to 0.01. Representative protein ID in each protein group was automatically selected using the in-house developed Leading tool (Raynaud et al., 2018).

Immunoprecipitation

Whole-cell extracts of K562 cells were prepared using lysis buffer (50 mM Tris-HCl pH 8, 150 mM NaCl, 5 mM EDTA pH8, 0.5% NP40) supplemented with protease inhibitor cocktail (Roche), 1mM PMSF, 1mM MgCl2 and Benzonase Nuclease 250 units/ 10 millions of cells (E1014-25KU, Sigma). Immunoprecipitations were performed overnight at 4°C with protein G Dynabeads (Thermo Fisher Scientific) coupled to either rabbit immunoglobulin G (IgG) (P120-201, Bethyl Laboratories) or rabbit ORC2 antibody (A302-734A, Bethyl Laboratories). Beads were washed 4 times with lysis buffer, then washed 3 times with 50 mM Tris HCl pH8. The immunoprecipitated complexes were eluted in 50 mM Tris HCl pH8 containing 1% SDS for 15 min à 56°C with agitation. IP samples were mixed with 1X Bolt Sample Reducing agent (Thermo Fisher Scientific) and 1X Bolt LDS Sample Buffer (Thermo Fisher Scientific), loaded and resolved on pre-cast Bolt Bis-Tris gels (Thermo Fisher Scientific), then transferred onto nitrocellulose membrane (GE Healthcare). Membranes were blocked in 5% fat-free milk in PBS, incubated overnight at 4°C with primary antibodies directed against ORC2 (A302-734A, Bethyl Laboratories) and GNL3 (sc-166460, Santa Cruz Biotechnology). A cognate secondary antibody coupled to horseradish peroxidase was used and revealed with the Super Signal West Dura Extended Duration Substrate kit (Thermo Fisher Scientific). Acquisition was performed using the Fusion FX (Vilber) and image analysis was performed using ImageJ (https://imagej.nih.gov/ij/).

Proteomics analysis of immunoprecipitation

Sample preparation: Tryptic peptides from the immunoprecipitated complexes (=eluate) were obtained by Strap Micro Spin Column according to the manufacturer's protocol (Protifi, NY, USA). Briefly: proteins from 140 µL of the eluate were diluted 1:1 with 2x reducing-alkylating buffer (20 mM TCEP, 100 mM

Chloroacetamide in 400 mM TEAB pH 8.5 and 4% SDS) and left 5 min at 95°C to allow reduction and alkylation in one step. Strap binding buffer was applied to precipitate proteins on quartz and proteolysis took place during 14 hrs at 37°C with 1 µg Trypsin sequencing grade (Promega). After speed-vacuum drying of eluted peptides, these were solubilized in 0.1% trifluoroacetic acid (TFA) in 10% Acetonitrile (ACN). Liquid Chromatography-coupled Mass spectrometry analysis (LC-MS): LC-MS analyses were performed on a Dionex U3000 HPLC nanoflow system coupled to a TIMS-TOF Pro mass spectrometer (Bruker Daltonik GmbH, Bremen, Germany). One µl was loaded, concentrated and washed for 3 min on a C18 reverse phase precolumn (3 µm particle size, 100 Å pore size, 75 µm inner diameter, 2 cm length, from Thermo Fisher Scientific). Peptides were separated on an Aurora C18 reverse phase resin (1.6 µm particle size, 100Å pore size, 75 µm inner diameter, 25 cm length mounted onto the Captive nanoSpray Ionization module, (IonOpticks, Middle Camberwell Australia) with a 60 minutes overall run-time gradient ranging from 99% of solvent A containing 0.1% formic acid in milliQ-grade H2O to 40% of solvent B containing 80% acetonitrile, 0.085% formic acid in mQH2O. The mass spectrometer acquired data throughout the elution process and operated in DDA PASEF mode with a 1.1 second/cycle, with Timed Ion Mobility Spectrometry (TIMS) mode enabled and a data-dependent scheme with full MS scans in PASEF mode. This enabled a recurrent loop analysis of a maximum of the 120 most intense nLC-eluting peptides which were CID-fragmented between each full scan every 1.1 second. Ion accumulation and ramp time in the dual TIMS analyzer were set to 50 ms each and the ion mobility range was set from 1/K0 = 0.6 Vs cm-2 to 1.6 Vs cm-2. Precursor ions for MS/MS analysis were isolated in positive mode with the PASEF mode set to « on » in the 100-1.700 m/z range by synchronizing quadrupole switching events with the precursor elution profile from the TIMS device. The cycle duty time was set to 100%, accommodating as many MSMS in the PASEF frame as possible. Singly charged precursor ions were excluded from the TIMS stage by tuning the TIMS using the otof control software, (Bruker Daltonik GmbH). Precursors for MS/MS were picked from an intensity threshold of 2.500 arbitrary units (a.u.) and resequenced until reaching a 'target value' of 20.000 a.u taking into account a dynamic exclusion of 0.40 s elution gap. Protein quantification and comparison : The mass spectrometry data were analyzed using Mascot version 2.5.1 (http://www.matrixscience.com/). The database used was a concatenation of Homo sapiens sequences from the Swissprot databases (release June 2020 : 563,972 sequences; 203,185,243 residues) and an in-house list of frequently found contaminant protein sequences. The enzyme specificity was trypsin's. The precursor and fragment mass tolerances were set to 20ppm. Oxidation of methionines was set as variable modifications while carbamidomethylation of cysteines was considered complete. False discovery rate

(FDR) was kept below 1% on both peptides and proteins. For comparative analysis, peptide count results from Mascot were assembled with the MyPROMS (Poullet et al., 2007) software (version 3.1).

References

Bauwens, S., Lototska, L., Koundrioukoff, S., Debatisse, M., Ye, J., Gilson, E., and Mendez-Bermudez, A. (2021). The Telomeric Protein TRF2 Regulates Replication Origin Activity within Pericentromeric Heterochromatin. Life (Basel) *11*.

Beck, H., Nähse-Kumpf, V., Larsen, M.S.Y., O'Hanlon, K.A., Patzke, S., Holmberg, C., Mejlvang, J., Groth, A., Nielsen, O., Syljuåsen, R.G.*, et al.* (2012). Cyclin-Dependent Kinase Suppression by WEE1 Kinase Protects the Genome through Control of Replication Initiation and Nucleotide Consumption. Molecular and Cellular Biology *32*, 4226-4236.

Bersaglieri, C., Kresoja-Rakic, J., Gupta, S., Bar, D., Kuzyakiv, R., Panatta, M., and Santoro, R. (2022). Genome-wide maps of nucleolus interactions reveal distinct layers of repressive chromatin domains. Nat Commun *13*, 1483.

Berti, M., Cortez, D., and Lopes, M. (2020). The plasticity of DNA replication forks in response to clinically relevant genotoxic stress. Nat Rev Mol Cell Biol *21*, 633-651.

Bialic, M., Coulon, V., Drac, M., Gostan, T., and Schwob, E. (2015). Analyzing the dynamics of DNA replication in Mammalian cells using DNA combing. Methods Mol Biol *1300*, 67-78.

Bianchi, J., Rudd, S.G., Jozwiakowski, S.K., Bailey, L.J., Soura, V., Taylor, E., Stevanovic, I., Green, A.J., Stracker, T.H., Lindsay, H.D.*, et al.* (2013). PrimPol bypasses UV photoproducts during eukaryotic chromosomal DNA replication. Mol Cell *52*, 566-573.

Blow, J.J., Ge, X.Q., and Jackson, D.A. (2011). How dormant origins promote complete genome replication. Trends Biochem Sci *36*, 405-414.

Coquel, F., Silva, M.J., Techer, H., Zadorozhny, K., Sharma, S., Nieminuszczy, J., Mettling, C., Dardillac, E., Barthe, A., Schmitz, A.L.*, et al.* (2018). SAMHD1 acts at stalled replication forks to prevent interferon induction. Nature *557*, 57-61.

Cornacchia, D., Dileep, V., Quivy, J.P., Foti, R., Tili, F., Santarella-Mellwig, R., Antony, C., Almouzni, G., Gilbert, D.M., and Buonomo, S.B. (2012). Mouse Rif1 is a key regulator of the replication-timing programme in mammalian cells. Embo J *31*, 3678-3690.

Courtot, L., Hoffmann, J.S., and Bergoglio, V. (2018). The Protective Role of Dormant Origins in Response to Replicative Stress. International journal of molecular sciences *19*.

Cox, J., and Mann, M. (2008). MaxQuant enables high peptide identification rates, individualized p.p.b.-range mass accuracies and proteome-wide protein quantification. Nature biotechnology *26*, 1367-1372.

Dungrawala, H., Rose, K.L., Bhat, K.P., Mohni, K.N., Glick, G.G., Couch, F.B., and Cortez, D. (2015). The Replication Checkpoint Prevents Two Types of Fork Collapse without Regulating Replisome Stability. Mol Cell *59*, 998-1010.

Elbaek, C.R., Petrosius, V., Benada, J., Erichsen, L., Damgaard, R.B., and Sorensen, C.S. (2022). WEE1 kinase protects the stability of stalled DNA replication forks by limiting CDK2 activity. Cell reports *38*, 110261.

Emerson, D.J., Zhao, P.A., Cook, A.L., Barnett, R.J., Klein, K.N., Saulebekova, D., Ge, C., Zhou, L., Simandi, Z., Minsk, M.K.*, et al.* (2022). Cohesin-mediated loop anchors confine the locations of human replication origins. Nature.

Fernandez-Vidal, A., Guitton-Sert, L., Cadoret, J.-C., Drac, M., Schwob, E., Baldacci, G., Cazaux, C., and Hoffmann, J.-S. (2014). A role for DNA polymerase θ in the timing of DNA replication. Nat Commun *5*, 4285.

Fragkos, M., Ganier, O., Coulombe, P., and Mechali, M. (2015). DNA replication origin activation in space and time. Nat Rev Mol Cell Biol *16*, 360-374.

Ge, X.Q., Jackson, D.A., and Blow, J.J. (2007). Dormant origins licensed by excess Mcm2-7 are required for human cells to survive replicative stress. Genes Dev *21*, 3331-3341.

Hadjadj, D., Denecker, T., Guérin, E., Kim, S.-J., Fauchereau, F., Baldacci, G., Maric, C., and Cadoret, J.-C. (2020). Efficient, quick and easy-to-use DNA replication timing analysis with START-R suite. NAR Genomics and Bioinformatics *2*.

Harrigan, J.A., Belotserkovskaya, R., Coates, J., Dimitrova, D.S., Polo, S.E., Bradshaw, C.R., Fraser, P., and Jackson, S.P. (2011). Replication stress induces 53BP1-containing OPT domains in G1 cells. The Journal of cell biology *193*, 97-108.

Hashimoto, Y., Chaudhuri, A.R., Lopes, M., and Costanzo, V. (2010). Rad51 protects nascent DNA from Mre11-dependent degradation and promotes continuous DNA synthesis. Nat Struct Mol Biol *17*, 1305-1311.

Hiratani, I., Ryba, T., Itoh, M., Yokochi, T., Schwaiger, M., Chang, C.-W., Lyou, Y., Townes, T.M., Schübeler, D., and Gilbert, D.M. (2008). Global Reorganization of Replication Domains During Embryonic Stem Cell Differentiation. PLOS Biology *6*, e245.

Holmberg Olausson, K., Nistér, M., and Lindström, M.S. (2014). Loss of nucleolar histone chaperone NPM1 triggers rearrangement of heterochromatin and synergizes with a deficiency in DNA methyltransferase DNMT3A to drive ribosomal DNA transcription. J Biol Chem *289*, 34601-34619.

Huang, C., Cheng, J., Bawa-Khalfe, T., Yao, X., Chin, Y.E., and Yeh, E.T.H. (2016). SUMOylated ORC2 Recruits a Histone Demethylase to Regulate Centromeric Histone Modification and Genomic Stability. Cell reports *15*, 147-157.

Huang, M., Itahana, K., Zhang, Y., and Mitchell, B.S. (2009). Depletion of guanine nucleotides leads to the Mdm2-dependent proteasomal degradation of nucleostemin. Cancer research *69*, 3004-3012.

Iarovaia, O.V., Minina, E.P., Sheval, E.V., Onichtchouk, D., Dokudovskaya, S., Razin, S.V., and Vassetzky, Y.S. (2019). Nucleolus: A Central Hub for Nuclear Functions. Trends Cell Biol *29*, 647-659.

Ibarra, A., Schwob, E., and Mendez, J. (2008). Excess MCM proteins protect human cells from replicative stress by licensing backup origins of replication. Proc Natl Acad Sci U S A *105*, 8956-8961.

Jones, M.J.K., Gelot, C., Munk, S., Koren, A., Kawasoe, Y., George, K.A., Santos, R.E., Olsen, J.V., McCarroll, S.A., Frattini, M.G.*, et al.* (2021). Human DDK rescues stalled forks and counteracts checkpoint inhibition at unfired origins to complete DNA replication. Mol Cell *81*, 426-441 e428.

Klein, K.N., Zhao, P.A., Lyu, X., Sasaki, T., Bartlett, D.A., Singh, A.M., Tasan, I., Zhang, M., Watts, L.P., Hiraga, S.I.*, et al.* (2021). Replication timing maintains the global epigenetic state in human cells. Science *372*, 371-378.

Kumbhar, R., Vidal-Eychenié, S., Kontopoulos, D.-G., Larroque, M., Larroque, C., Basbous, J., Kossida, S., Ribeyre, C., and Constantinou, A. (2018). Recruitment of ubiquitin-activating enzyme UBA1 to DNA by poly(ADP-ribose) promotes ATR signalling. Life Science Alliance *1*.

Lambert, S., and Carr, A.M. (2013). Impediments to replication fork movement: stabilisation, reactivation and genome instability. Chromosoma *122*, 33-45.

Liao, H., Ji, F., Helleday, T., and Ying, S. (2018). Mechanisms for stalled replication fork stabilization: new targets for synthetic lethality strategies in cancer treatments. EMBO reports *19*, e46263.

Lin, T., Ibrahim, W., Peng, C.Y., Finegold, M.J., and Tsai, R.Y. (2013). A novel role of nucleostemin in maintaining the genome integrity of dividing hepatocytes during mouse liver development and regeneration. Hepatology *58*, 2176-2187.

Lin, T., Meng, L., Lin, T.C., Wu, L.J., Pederson, T., and Tsai, R.Y. (2014). Nucleostemin and GNL3L exercise distinct functions in genome protection and ribosome synthesis, respectively. J Cell Sci *127*, 2302-2312.

Lossaint, G., Larroque, M., Ribeyre, C., Bec, N., Larroque, C., Decaillet, C., Gari, K., and Constantinou, A. (2013). FANCD2 binds MCM proteins and controls replisome function upon activation of s phase checkpoint signaling. Mol Cell *51*, 678-690.

MacAlpine, H.K., Gordan, R., Powell, S.K., Hartemink, A.J., and MacAlpine, D.M. (2010). Drosophila ORC localizes to open chromatin and marks sites of cohesin complex loading. Genome research *20*, 201-211.

Macheret, M., and Halazonetis, T.D. (2015). DNA replication stress as a hallmark of cancer. Annu Rev Pathol *10*, 425-448.

Maida, Y., Yasukawa, M., Okamoto, N., Ohka, S., Kinoshita, K., Totoki, Y., Ito, T.K., Minamino, T., Nakamura, H., Yamaguchi, S.*, et al.* (2014). Involvement of telomerase reverse transcriptase in heterochromatin maintenance. Mol Cell Biol *34*, 1576-1593.

Mechali, M. (2010). Eukaryotic DNA replication origins: many choices for appropriate answers. Nat Rev Mol Cell Biol *11*, 728-738.

Meng, L., Lin, T., Peng, G., Hsu, J.K., Lee, S., Lin, S.Y., and Tsai, R.Y. (2013). Nucleostemin deletion reveals an essential mechanism that maintains the genomic stability of stem and progenitor cells. Proc Natl Acad Sci U S A *110*, 11415-11420.

Meng, L., Yasumoto, H., and Tsai, R.Y. (2006). Multiple controls regulate nucleostemin partitioning between nucleolus and nucleoplasm. J Cell Sci *119*, 5124-5136.

Meng, L., Zhu, Q., and Tsai, R.Y. (2007). Nucleolar trafficking of nucleostemin family proteins: common versus protein-specific mechanisms. Mol Cell Biol *27*, 8670-8682.

Mier, P., Perez-Pulido, A.J., Reynaud, E.G., and Andrade-Navarro, M.A. (2017). Reading the Evolution of Compartmentalization in the Ribosome Assembly Toolbox: The YRG Protein Family. PloS one *12*, e0169750.

Minocherhomji, S., Ying, S., Bjerregaard, V.A., Bursomanno, S., Aleliunaite, A., Wu, W., Mankouri, H.W., Shen, H., Liu, Y., and Hickson, I.D. (2015). Replication stress activates DNA repair synthesis in mitosis. Nature *528*, 286-290.

Miotto, B., Ji, Z., and Struhl, K. (2016). Selectivity of ORC binding sites and the relation to replication timing, fragile sites, and deletions in cancers. Proceedings of the National Academy of Sciences *113*, E4810-E4819.

Moiseeva, T.N., Qian, C., Sugitani, N., Osmanbeyoglu, H.U., and Bakkenist, C.J. (2019). WEE1 kinase inhibitor AZD1775 induces CDK1 kinase-dependent origin firing in unperturbed G1- and S-phase cells. Proceedings of the National Academy of Sciences *116*, 23891-23893.

Ohta, S., Tatsumi, Y., Fujita, M., Tsurimoto, T., and Obuse, C. (2003). The ORC1 cycle in human cells: II. Dynamic changes in the human ORC complex during the cell cycle. J Biol Chem *278*, 41535-41540.

Oktar, P.A., Yildirim, S., Balci, D., and Can, A. (2011). Continual Expression Throughout the Cell Cycle and Downregulation upon Adipogenic Differentiation Makes Nucleostemin a Vital Human MSC Proliferation Marker. Stem Cell Reviews and Reports *7*, 413-424.

Padeken, J., Mendiburo, M.J., Chlamydas, S., Schwarz, H.J., Kremmer, E., and Heun, P. (2013). The nucleoplasmin homolog NLP mediates centromere clustering and anchoring to the nucleolus. Mol Cell *50*, 236-249.

Peng, M., Cong, K., Panzarino, N.J., Nayak, S., Calvo, J., Deng, B., Zhu, L.J., Morocz, M., Hegedus, L., Haracska, L.*, et al.* (2018). Opposing Roles of FANCJ and HLTF Protect Forks and Restrain Replication during Stress. Cell reports *24*, 3251-3261.

Poullet, P., Carpentier, S., and Barillot, E. (2007). myProMS, a web server for management and validation of mass spectrometry-based proteomic data. Proteomics *7*, 2553-2556.

Prasanth, S.G., Prasanth, K.V., Siddiqui, K., Spector, D.L., and Stillman, B. (2004). Human Orc2 localizes to centrosomes, centromeres and heterochromatin during chromosome inheritance. EMBO J *23*, 2651-2663.

Prigent, C., and Dimitrov, S. (2003). Phosphorylation of serine 10 in histone H3, what for? J Cell Sci *116*, 3677-3685.

Quiroga-Artigas, G., de Jong, D., and Schnitzler, C.E. (2022). GNL3 is an evolutionarily conserved stem cell gene influencing cell proliferation, animal growth and regeneration in the hydrozoan Hydractinia. Open Biol *12*, 220120.

Raynaud, F., Homburger, V., Seveno, M., Vigy, O., Moutin, E., Fagni, L., and Perroy, J. (2018). SNAP23-Kif5 complex controls mGlu1 receptor trafficking. Journal of molecular cell biology *10*, 423-436.

Reynaud, E.G., Andrade, M.A., Bonneau, F., Ly, T.B., Knop, M., Scheffzek, K., and Pepperkok, R. (2005). Human Lsg1 defines a family of essential GTPases that correlates with the evolution of compartmentalization. BMC Biol *3*, 21.

Ribeyre, C., Lebdy, R., Patouillard, J., Larroque, M., Abou-Merhi, R., Larroque, C., and Constantinou, A. (2021). The organizer of chromatin topology RIF1 ensures cellular resilience to DNA replication stress. bioRxiv, 669234.

Ribeyre, C., Zellweger, R., Chauvin, M., Bec, N., Larroque, C., Lopes, M., and Constantinou, A. (2016). Nascent DNA Proteomics Reveals a Chromatin Remodeler Required for Topoisomerase I Loading at Replication Forks. Cell reports *15*, 300-309.

Rickman, K., and Smogorzewska, A. (2019). Advances in understanding DNA processing and protection at stalled replication forks. The Journal of cell biology *218*, 1096-1107.

Roux, K.J., Kim, D.I., Raida, M., and Burke, B. (2012). A promiscuous biotin ligase fusion protein identifies proximal and interacting proteins in mammalian cells. The Journal of cell biology *196*, 801-810.

Sasi, N.K., Coquel, F., Lin, Y.L., MacKeigan, J.P., Pasero, P., and Weinreich, M. (2018). DDK Has a Primary Role in Processing Stalled Replication Forks to Initiate Downstream Checkpoint Signaling. Neoplasia *20*, 985-995.

Schiavone, D., Jozwiakowski, S.K., Romanello, M., Guilbaud, G., Guilliam, T.A., Bailey, L.J., Sale, J.E., and Doherty, A.J. (2016). PrimPol Is Required for Replicative Tolerance of G Quadruplexes in Vertebrate Cells. Mol Cell *61*, 161-169.

Schlacher, K., Christ, N., Siaud, N., Egashira, A., Wu, H., and Jasin, M. (2011). Double-strand break repair-independent role for BRCA2 in blocking stalled replication fork degradation by MRE11. Cell *145*, 529-542.

Schlacher, K., Wu, H., and Jasin, M. (2012). A distinct replication fork protection pathway connects Fanconi anemia tumor suppressors to RAD51-BRCA1/2. Cancer cell *22*, 106-116.

Schumacher, B., Pothof, J., Vijg, J., and Hoeijmakers, J.H.J. (2021). The central role of DNA damage in the ageing process. Nature *592*, 695-703.

Schwab, R.A., Nieminuszczy, J., Shin-ya, K., and Niedzwiedz, W. (2013). FANCJ couples replication past natural fork barriers with maintenance of chromatin structure. The Journal of cell biology *201*, 33-48.

Shibata, E., Kiran, M., Shibata, Y., Singh, S., Kiran, S., and Dutta, A. (2016). Two subunits of human ORC are dispensable for DNA replication and proliferation. Elife *5*.

Shimada, K., and Gasser, S.M. (2007). The origin recognition complex functions in sister-chromatid cohesion in Saccharomyces cerevisiae. Cell *128*, 85-99.

Sobecki, M., Mrouj, K., Camasses, A., Parisis, N., Nicolas, E., Llères, D., Gerbe, F., Prieto, S., Krasinska, L., David, A.*, et al.* (2016). The cell proliferation antigen Ki-67 organises heterochromatin. Elife *5*, e13722.

Soniat, M.M., Myler, L.R., Kuo, H.C., Paull, T.T., and Finkelstein, I.J. (2019). RPA Phosphorylation Inhibits DNA Resection. Mol Cell *75*, 145-153 e145.

Stenstrom, L., Mahdessian, D., Gnann, C., Cesnik, A.J., Ouyang, W., Leonetti, M.D., Uhlen, M., Cuylen-Haering, S., Thul, P.J., and Lundberg, E. (2020). Mapping the nucleolar proteome reveals a spatiotemporal organization related to intrinsic protein disorder. Mol Syst Biol *16*, e9469.

Toledo, L.I., Altmeyer, M., Rask, M.B., Lukas, C., Larsen, D.H., Povlsen, L.K., Bekker-Jensen, S., Mailand, N., Bartek, J., and Lukas, J. (2013). ATR prohibits replication catastrophe by preventing global exhaustion of RPA. Cell *155*, 1088-1103.

Tsai, R.Y. (2014). Turning a new page on nucleostemin and self-renewal. J Cell Sci *127*, 3885-3891.

Tsai, R.Y., and McKay, R.D. (2002). A nucleolar mechanism controlling cell proliferation in stem cells and cancer cells. Genes Dev *16*, 2991-3003.

Tsai, R.Y., and McKay, R.D. (2005). A multistep, GTP-driven mechanism controlling the dynamic cycling of nucleostemin. The Journal of cell biology *168*, 179-184.

Tyanova, S., Temu, T., Sinitcyn, P., Carlson, A., Hein, M.Y., Geiger, T., Mann, M., and Cox, J. (2016). The Perseus computational platform for comprehensive analysis of (prote)omics data. Nature methods *13*, 731-740.

Wang, W., Klein, K.N., Proesmans, K., Yang, H., Marchal, C., Zhu, X., Borrman, T., Hastie, A., Weng, Z., Bechhoefer, J.*, et al.* (2021). Genome-wide mapping of human DNA replication by optical replication mapping supports a stochastic model of eukaryotic replication. Molecular Cell *81*, 2975-2988.e2976.

Wong, L.H., Brettingham-Moore, K.H., Chan, L., Quach, J.M., Anderson, M.A., Northrop, E.L., Hannan, R., Saffery, R., Shaw, M.L., Williams, E.*, et al.* (2007). Centromere RNA is a key component for the assembly of nucleoproteins at the nucleolus and centromere. Genome research *17*, 1146-1160.

Yamashita, M., Nitta, E., Nagamatsu, G., Ikushima, Y.M., Hosokawa, K., Arai, F., and Suda, T. (2013). Nucleostemin is indispensable for the maintenance and genetic stability of hematopoietic stem cells. Biochem Biophys Res Commun *441*, 196-201.

Yamazaki, S., Ishii, A., Kanoh, Y., Oda, M., Nishito, Y., and Masai, H. (2012). Rif1 regulates the replication timing domains on the human genome. EMBO J *31*, 3667-3677.

Zellweger, R., Dalcher, D., Mutreja, K., Berti, M., Schmid, J.A., Herrador, R., Vindigni, A., and Lopes, M. (2015). Rad51-mediated replication fork reversal is a global response to genotoxic treatments in human cells. The Journal of cell biology *208*, 563-579.

Zeman, M.K., and Cimprich, K.A. (2014). Causes and consequences of replication stress. Nat Cell Biol *16*, 2-9.

Figure 1

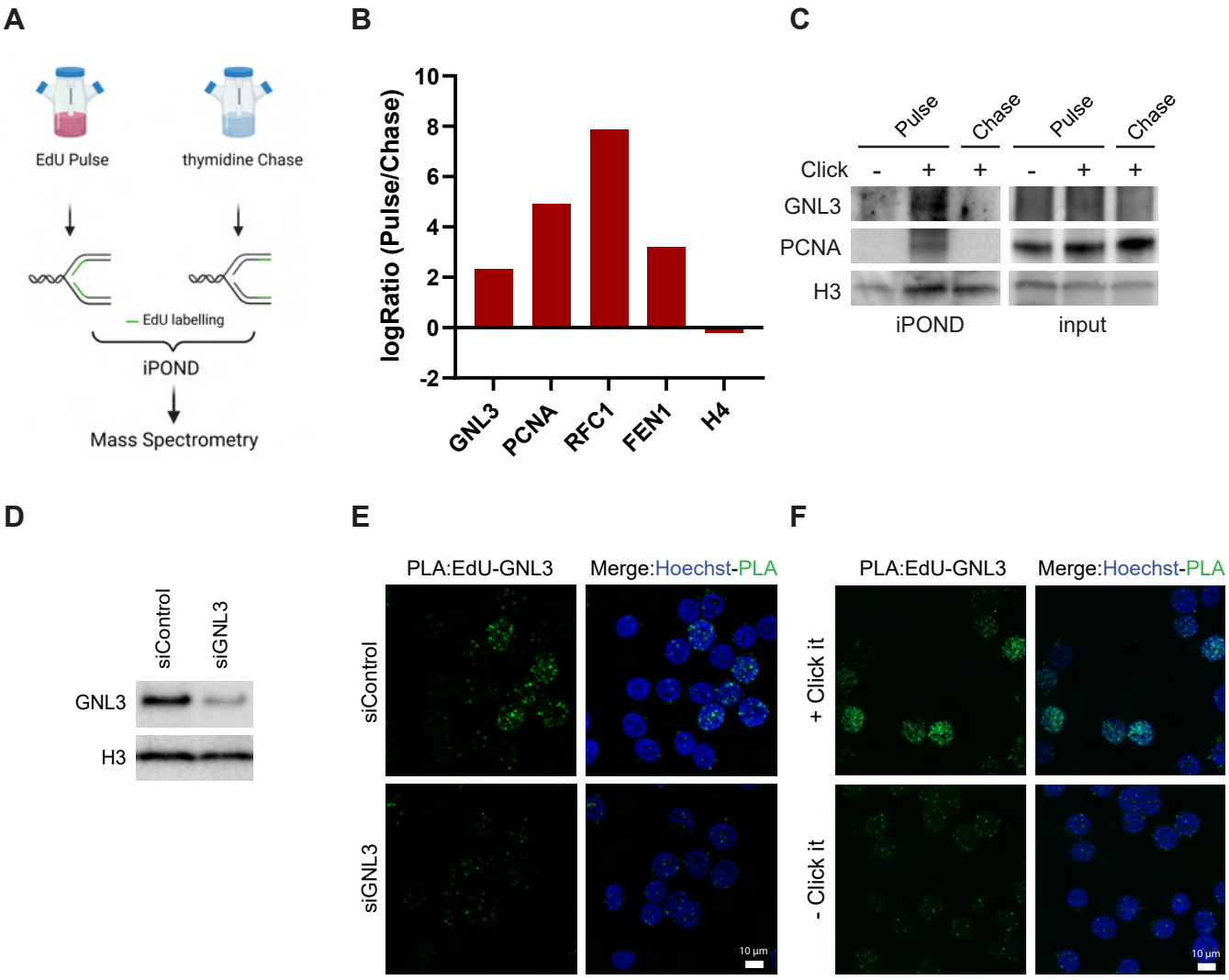
A
EdU Pulse
thymidine Chase
EdU labelling
iPOND
Mass Spectrometry
B
logRatio (Pulse/Chase)
10
8
6
4
2
0
-2
GNL3
PCNA
RFC1
FEN1
H4
C
Pulse
Chase
Pulse
Chase
Click
-
+
+
-
+
+
GNL3
PCNA
H3
iPOND
input
D
siControl
siGNL3
GNL3
H3
E
PLA:EdU-GNL3
Merge:Hoechst-PLA
siControl
siGNL3
10 µm
F
PLA:EdU-GNL3
Merge:Hoechst-PLA
+ Click it
- Click it
10 µm

Figure 2

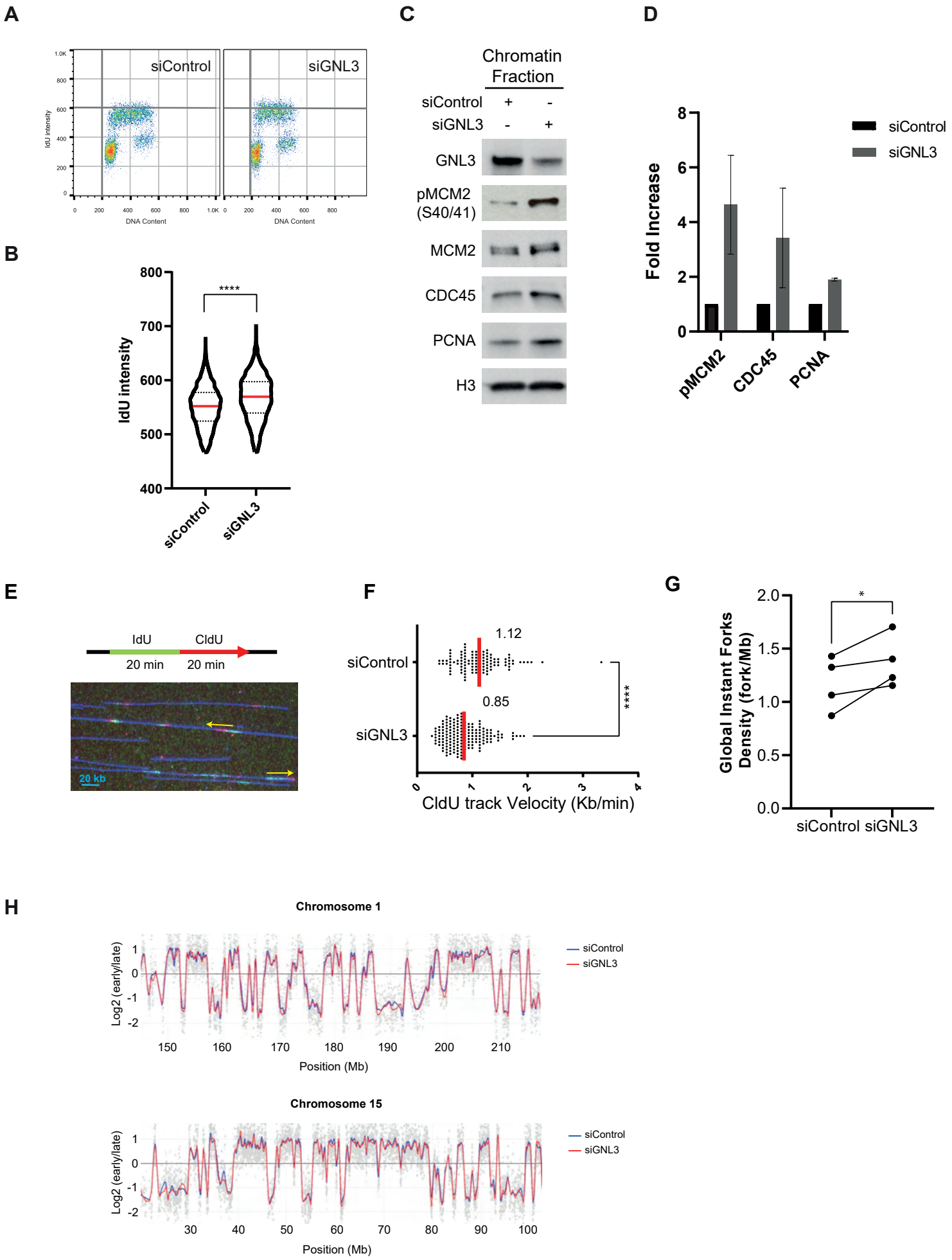
A
siControl
siGNL3
IdU intensity
DNA Content
B
IdU intensity
****
siControl
siGNL3
C
Chromatin Fraction
siControl + -
siGNL3 - +
GNL3
pMCM2 (S40/41)
MCM2
CDC45
PCNA
H3
D
Fold Increase
siControl
siGNL3
pMCM2
CDC45
PCNA
E
IdU
CldU
20 min
20 min
20 kb
F
siControl
siGNL3
1.12
0.85
****
CldU track Velocity (Kb/min)
G
Global Instant Forks Density (fork/Mb)
*
siControl siGNL3
H
Chromosome 1
Log2 (early/late)
Position (Mb)
siControl
siGNL3
Chromosome 15
Log2 (early/late)
Position (Mb)
siControl
siGNL3

Figure 3

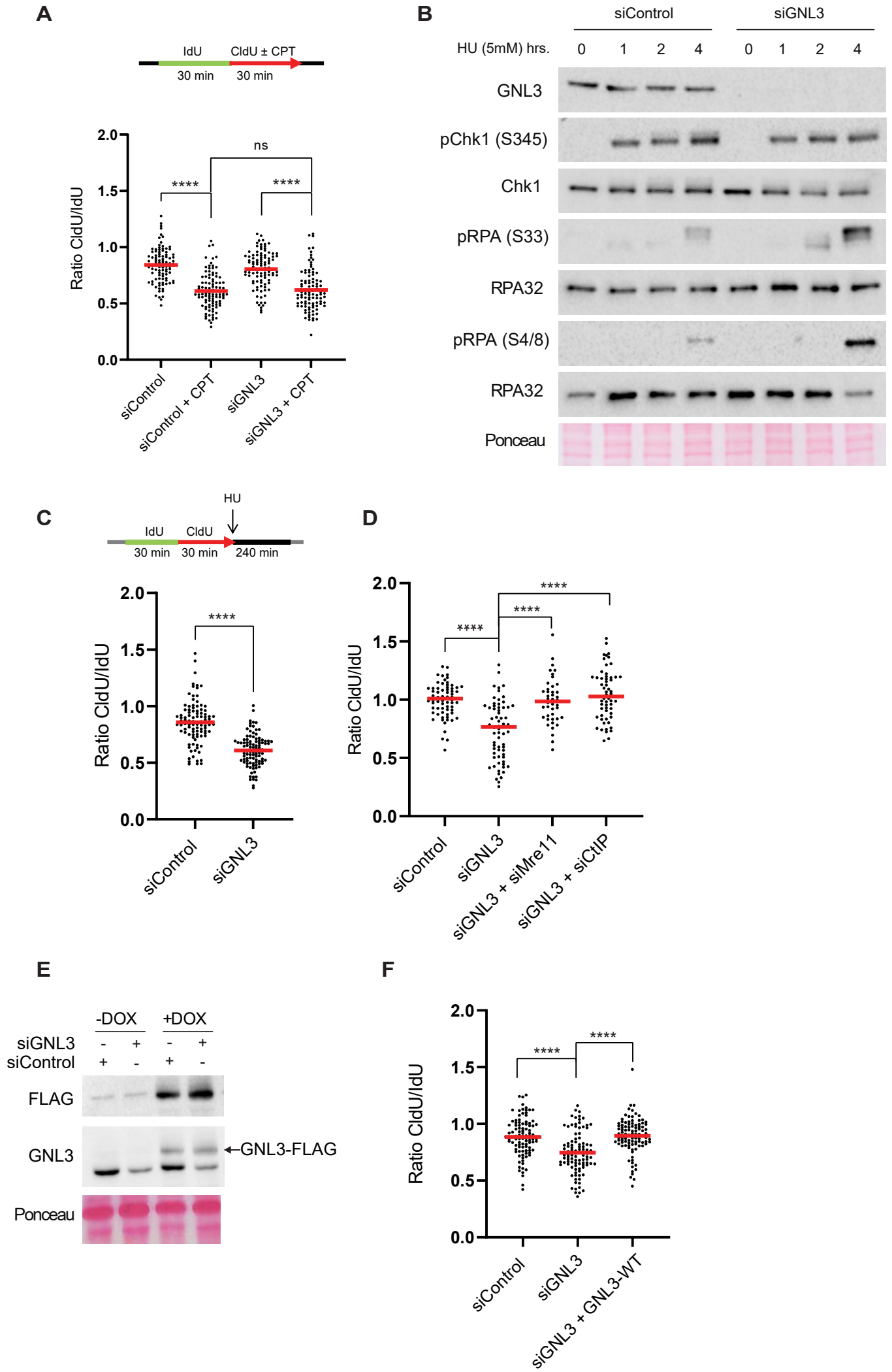
A
IdU
CldU ± CPT
30 min
30 min
Ratio CldU/IdU
2.0
1.5
1.0
0.5
0.0
ns
****
****
siControl
siControl + CPT
siGNL3
siGNL3 + CPT
B
siControl
siGNL3
HU (5mM) hrs.
0 1 2 4 0 1 2 4
GNL3
pChk1 (S345)
Chk1
pRPA (S33)
RPA32
pRPA (S4/8)
RPA32
Ponceau
C
HU
IdU
CldU
30 min
30 min
240 min
Ratio CldU/IdU
****
siControl
siGNL3
D
Ratio CldU/IdU
****
****
****
siControl
siGNL3
siGNL3 + siMre11
siGNL3 + siCtIP
E
-DOX
+DOX
siGNL3
siControl
FLAG
GNL3
←GNL3-FLAG
Ponceau
F
Ratio CldU/IdU
****
****
siControl
siGNL3
siGNL3 + GNL3-WT

Figure 4

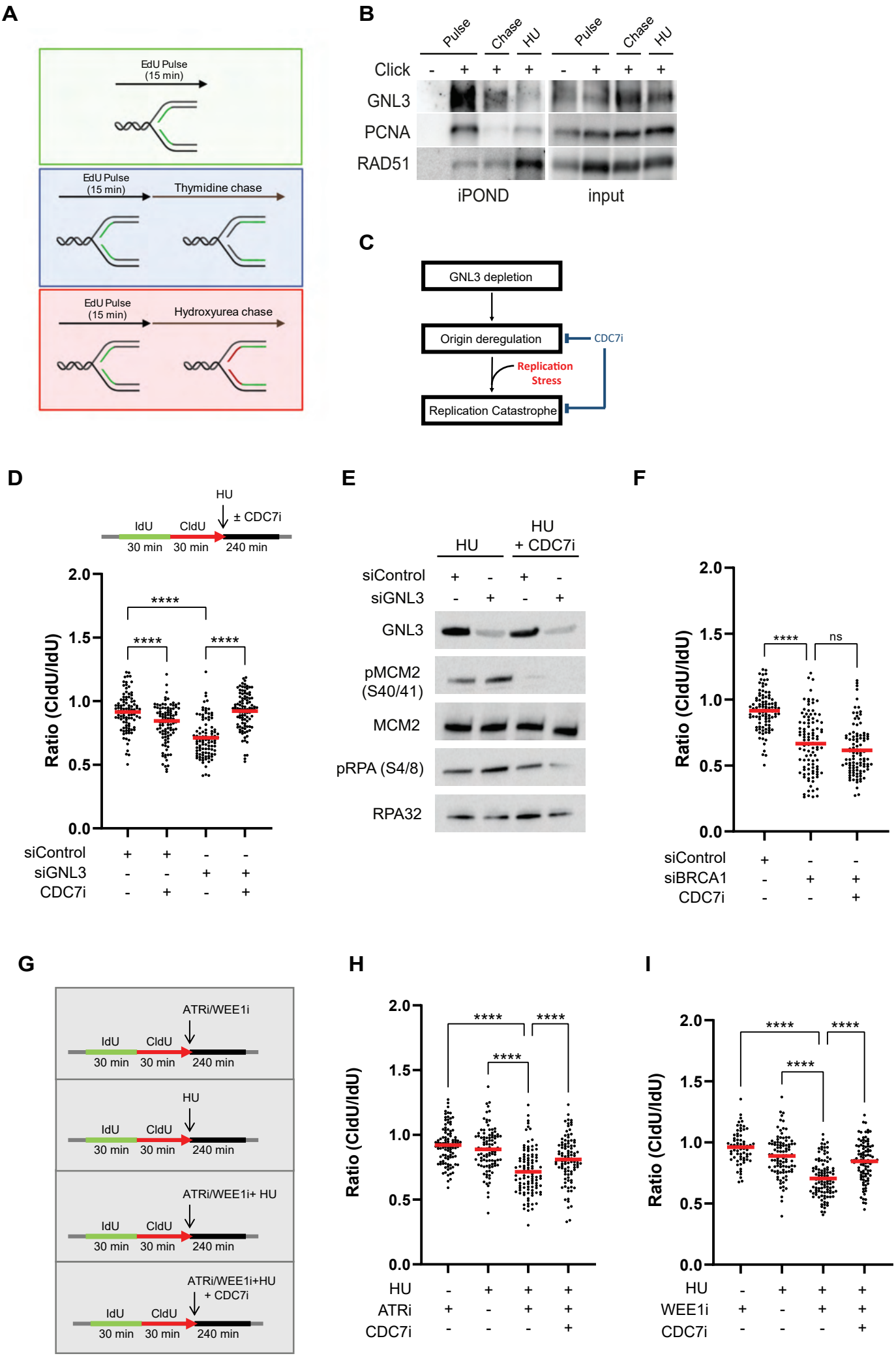
A
EdU Pulse (15 min)
EdU Pulse (15 min)
Thymidine chase
EdU Pulse (15 min)
Hydroxyurea chase
B
Pulse
Chase
HU
Pulse
Chase
HU
Click
GNL3
PCNA
RAD51
iPOND
input
C
GNL3 depletion
Origin deregulation
CDC7i
Replication Stress
Replication Catastrophe
D
HU
± CDC7i
IdU
CldU
30 min
30 min
240 min
Ratio (CldU/IdU)
siControl
siGNL3
CDC7i
E
HU
HU + CDC7i
siControl
siGNL3
GNL3
pMCM2 (S40/41)
MCM2
pRPA (S4/8)
RPA32
F
Ratio (CldU/IdU)
ns
siControl
siBRCA1
CDC7i
G
ATRi/WEE1i
HU
ATRi/WEE1i+ HU
ATRi/WEE1i+HU + CDC7i
IdU
CldU
30 min
30 min
240 min
H
Ratio (CldU/IdU)
HU
ATRi
CDC7i
I
Ratio (CldU/IdU)
HU
WEE1i
CDC7i

Figure 5

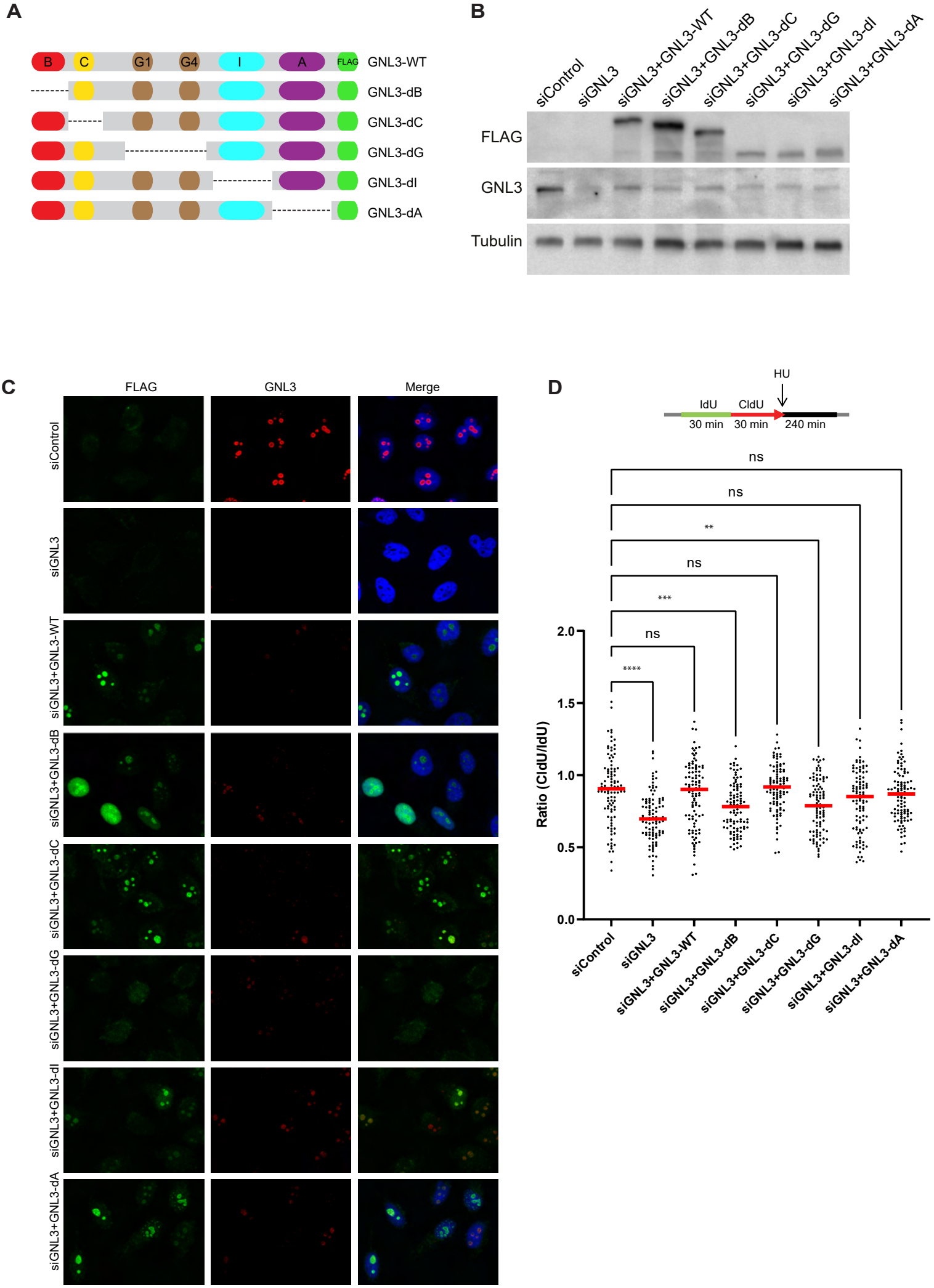
A
B
C
G1
G4
I
A
FLAG
GNL3-WT
GNL3-dB
GNL3-dC
GNL3-dG
GNL3-dI
GNL3-dA
B
siControl
siGNL3
siGNL3+GNL3-WT
siGNL3+GNL3-dB
siGNL3+GNL3-dC
siGNL3+GNL3-dG
siGNL3+GNL3-dI
siGNL3+GNL3-dA
FLAG
GNL3
Tubulin
C
FLAG
GNL3
Merge
siControl
siGNL3
siGNL3+GNL3-WT
siGNL3+GNL3-dB
siGNL3+GNL3-dC
siGNL3+GNL3-dG
siGNL3+GNL3-dI
siGNL3+GNL3-dA
D
HU
IdU
CldU
30 min
30 min
240 min
ns
ns
**
ns
***
ns
****
Ratio (CldU/IdU)
2.0
1.5
1.0
0.5
0.0
siControl
siGNL3
siGNL3+GNL3-WT
siGNL3+GNL3-dB
siGNL3+GNL3-dC
siGNL3+GNL3-dG
siGNL3+GNL3-dI
siGNL3+GNL3-dA

Figure 6

A

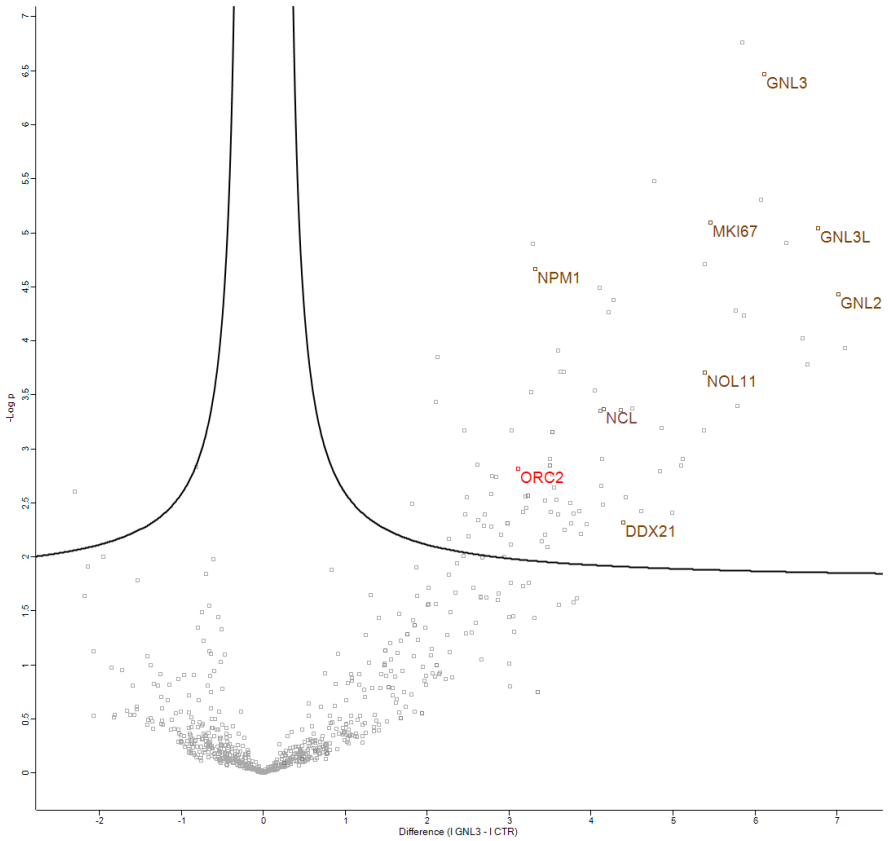

B

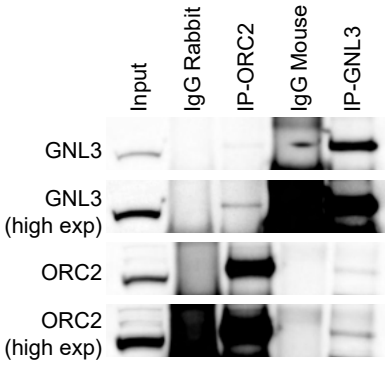

C

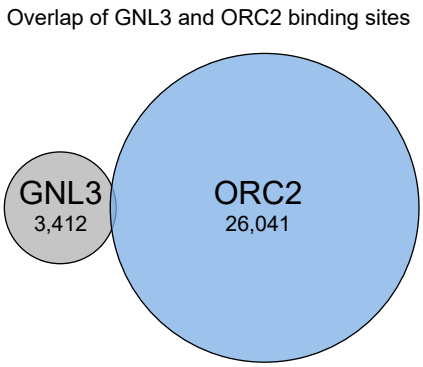

D

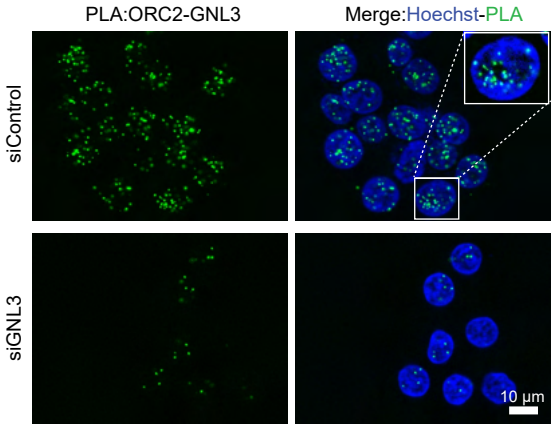

Figure 7

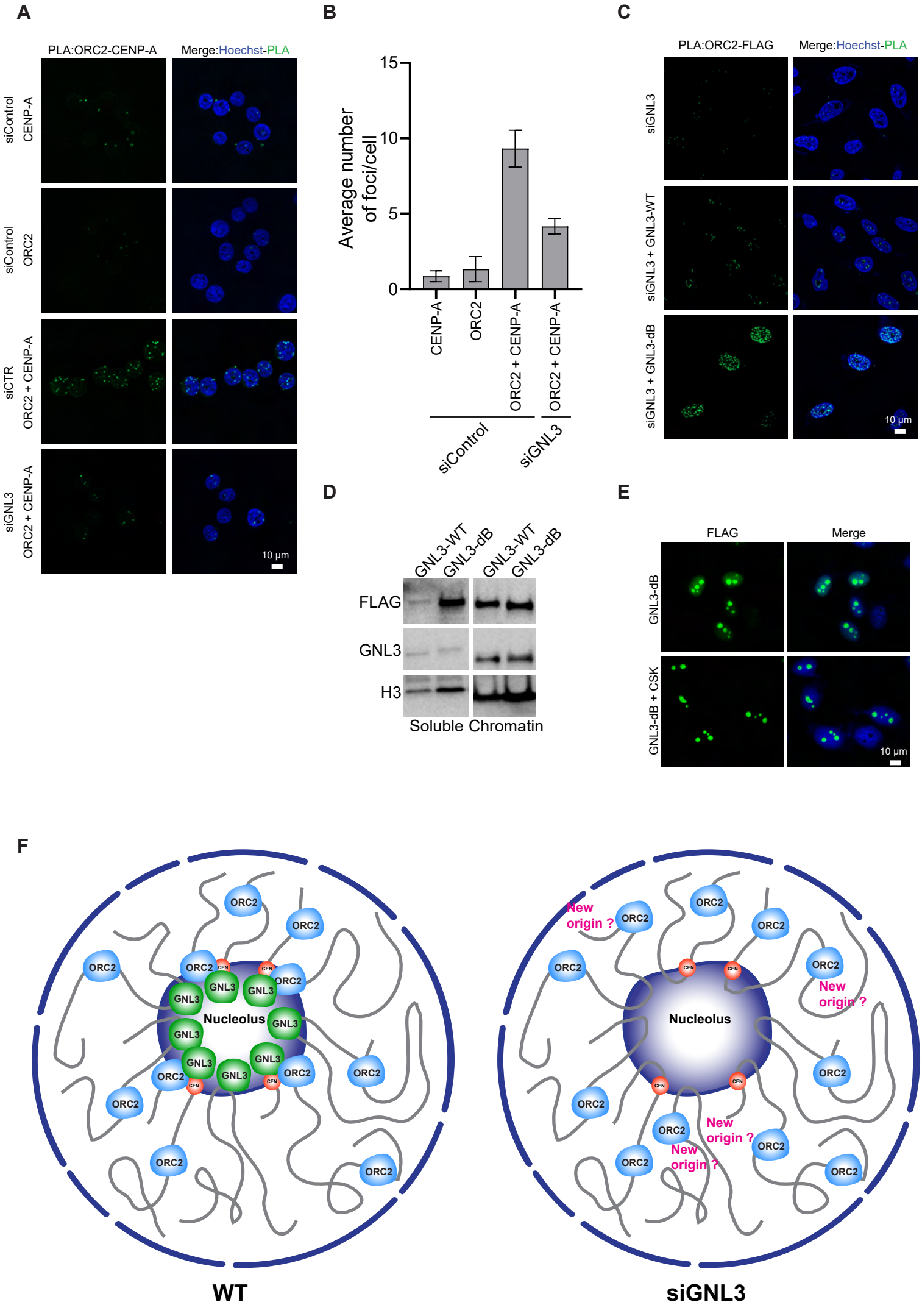
A
PLA:ORC2-CENP-A
Merge:Hoechst-PLA
siControl CENP-A
siControl ORC2
siCTR ORC2 + CENP-A
siGNL3 ORC2 + CENP-A
10 µm
B
Average number of foci/cell
15
10
5
0
CENP-A
ORC2
ORC2 + CENP-A
ORC2 + CENP-A
siControl
siGNL3
C
PLA:ORC2-FLAG
Merge:Hoechst-PLA
siGNL3
siGNL3 + GNL3-WT
siGNL3 + GNL3-dB
10 µm
D
GNL3-WT
GNL3-dB
GNL3-WT
GNL3-dB
FLAG
GNL3
H3
Soluble
Chromatin
E
FLAG
Merge
GNL3-dB
GNL3-dB + CSK
10 µm
F
ORC2
GNL3
CEN
Nucleolus
New origin ?
WT
siGNL3